PREDICTING SPATIAL SMOOTHING FOR SOLAR PV POWER USING THE WAVELET VARIABILITY MODEL

by Ana Dyreson

A Thesis

Submitted in Partial Fulfillment

of the Requirements for the Degree of

Master of Science

in Mechanical Engineering

Northern Arizona University

May, 2014

Approved:

Tom Acker, Ph.D., Chair

Michael Shafer, Ph.D.

Peter Vadasz, D.Sc.

Eric Morgan, Ph.D.

www.manaraa.com

UMI Number: 1556716

All rights reserved

INFORMATION TO ALL USERS
The quality of this reproduction is dependent upon the quality of the copy submitted.

In the unlikely event that the author did not send a complete manuscript
and there are missing pages, these will be noted. Also, if material had to be removed,
a note will indicate the deletion.

UMI 1556716

Published by ProQuest LLC (2014). Copyright in the Dissertation held by the Author.

Microform Edition © ProQuest LLC.
All rights reserved. This work is protected against
unauthorized copying under Title 17, United States Code

ProQuest LLC.
789 East Eisenhower Parkway
P.O. Box 1346
Ann Arbor, MI 48106 - 1346

www.manaraa.com

ABSTRACT

Predicting Spatial Smoothing for Solar PV Power using the Wavelet Variability Model

Ana Dyreson

Solar photovoltaic (PV) power plants produce power in proportion to the incoming power density of sunlight. This available power (irradiance) is variable due to the motion of passing clouds. With increasing penetrations of solar PV power in the electricity grid, the variability of the irradiance is important to understand because variable resources can challenge grid operations by causing voltage fluctuations and increasing the cost of maintaining the overall energy supply and demand balance that is essential to a stable power grid.

Irradiance measured at a single sensor is often used to predict the power output of a PV power plant and plan for the variability effects on the grid. However, it is known that irradiance measured at a single point is not representative of the output of a PV power plant directly, since a PV power plant receives incoming irradiance over a large area. The integrated or averaged irradiance over the area of the plant is less variable than a single point. This thesis seeks to understand what smoothing occurs over a power plant area, how many irradiance sensors are required to measure the smoothed irradiance, and what frequency of data collection is required.

The smoothing of solar irradiance over the extent of PV power plants is examined using two methods: averaging measurements from many irradiance sensors, and using a model developed by Lave, Kleissl, and Stein [1] called the Wavelet Variability Model (WVM). This thesis utilizes data from a network of 45 solar irradiance sensors which was deployed north

www.manaraa.com

of Flagstaff, AZ. The results show the similarities and differences between two irradiance smoothing methods. These two models both show that the smoothing effect is significant for large PV power plants, which means the power plant output has less variability and is easier to integrate into the electricity grid than might have been expected using a single point sensor measurement to predict variability. Both also show that, as expected, the smoothing effect increases as power plant size increases. A comparison of the ramp distributions between the two models shows that the WVM predicts many fewer ramps overall when compared to averaging the irradiance measurements, and virtually eliminates all of the ramps under a few seconds. Although validation against actual power plant output was not possible at this site, the WVM's prediction of fewer, longer ramps would be more favorable from a grid integration perspective and so is a promising result. In addition, the ability of the WVM to handle irradiance smoothing differently depending on the cloud conditions of individual days was explored and a strength of the model. Using the WVM, this thesis proposes that a five sensor network is sufficient to model the smoothed irradiance and that the irradiance should be measured at one second frequency to accurately model the variability. These results shed light on the spatial smoothing of irradiance, and suggest further work in comparing actual power output to the irradiance smoothing models in order to select an irradiance smoothing model that is most representative of actual PV power plant output variability.

www.manaraa.com

Acknowledgments

My graduate project is just one piece of a multi-year wind and solar variability study which involved industry partners (NextEra Energy Resources, WindLogics, and Babbitt Ranches) as well as at least ten staff and students at NAU. This team worked together in creating this project, designing the data collection hardware, and working in the field collecting data. All of those efforts are appreciated. I would like to thank in particular Tom Acker for lending his wisdom and leadership, and Eric Morgan for his abundance of ideas and many hours of advising on this project. Sam Monger was my colleague and partner in this project and I thank him for being an good teammate and friend and in particular for all of the weekends he spent in the field collecting data. David Willy was also a major contributor to this project both before I was in graduate school and after, and I always appreciate his experience and advice. Finally, my husband Devon is the partner in all the adventures in my life including moving to Flagstaff to start a graduate program. Were it not for him I wouldn't have been on a six month road trip that lead us to Flagstaff together, opening the doors to graduate school and a whole new career studying solar energy, which is another adventure he is thankfully willing to support me in.

www.manaraa.com

Contents

www.manaraa.com

www.manaraa.com

List of Tables

www.manaraa.com

www.manaraa.com

List of Figures

www.manaraa.com

www.manaraa.com

www.manaraa.com

www.manaraa.com

Table 0.1: Nomenclature and Abbreviations, In order of appearance

Symbol or Abbreviation	Description
k_t	Clearness index
VI	Variability Index
CSI	Clear sky index
GHI	Global horizontal irradiance
I	Plane-of-array irradiance
C	Constant = 1000 W/m^2
$DARR$	Daily aggregate ramp rate
Ψ	Wavelet function
λ	Timescale in wavelet analysis
A	Average value
D	Difference between two subsequent averages
β	Step function representing D
W^H	Wavelet coefficients
I^H	Wavelet periodogram values
T_j	Characteristic persistence
cf_p, fpi	Fluctation power index
cf_e	Fluctation energy index
VR	Variability reduction
N	Number of sites
ρ	Correlation coefficient
A	Correlation scaling coefficient or A value
$d_{m,n}$	Distance between two sites
MBE	Mean bias error
$RMSE$	Root mean square error
NVI	Natural Variability of Irradiance
TL	Linke Turbidity
δ	Optical thickness
B_{nc}	Clear sky beam normal irradiance
I_o	Solar constant
AM	Air mass

www.manaraa.com

Chapter 1

Introduction

1.1 Motivation

Electrical energy generation in the US has historically come from non-variable generation sources - largely fossil fuels, hydroelectricity, and nuclear [2]. These energy sources are considered non-variable because output is controlled by the operator and so can be turned on, off, or modulated as needed (subject to some physical limitations, of course, but largely controllable on demand). Variable generation sources such as wind and solar photovoltaics, in contrast, may be ramped down as needed but their upper limit of available power is subject to the availability of the solar and wind resources at a given time. Variable sources such as wind and solar power are increasingly contributing to electricity generation in the US. Solar photovoltaic (PV) and wind sources contributed an essentially negligible amount to overall electricity generation in 1985 (17 million kWh generated out of a total of about 2,500 billion kWh in the US), but grew to 3.7 percent of energy served in 2012 [3]. The contribution of renewable energy sources, especially solar and wind, to electricity generation is projected to grow faster than that of fossil fuels through 2040 [4].

The stability of the electricity grid is impacted by changes in generation or load

www.manaraa.com

that are not anticipated by operators, such as large increases or decreases in power provided by variable generation sources. The system must be prepared and physically capable of responding to this variability.

This work considers the variability of solar PV. Solar PV power plants are variable generation sources because of the entirely predictable motion of the sun through the sky, which causes increasing power in the morning hours and decreasing in the afternoon. In addition solar PV power plants are variable because of the less predictable, shorter timescale effects of clouds. The less predictable component of variability is of interest to grid operators and is the focus of this work. Cloud motion over a single irradiance sensor can show large changes in irradiance on a second-to-second basis. If this represented the variability of a large PV power plant, and if many of such generators existed on the grid, it would negatively affect the stability of the grid. In reality, though, as clouds move over a PV plant, each PV module is impacted at a different time, depending on the location of the module and cloud characteristics. This is referred to as spatial smoothing and it results in less variability of the true power plant output than of the single point irradiance measurement. The irradiance averaged over the area of the power plant footprint will have smaller fluctuations in irradiance than the irradiance point sensor. Since power is approximately proportional to aggregate irradiance [5], the power plant's power fluctuations are expected to be proportional to the smaller, spatially smoothed fluctuations, not the fluctuations from a single point sensor.

Spatial smoothing is illustrated in Figure 1.1 which shows irradiance measurements over the course of a day and Figure 1.2 which shows irradiance measurements over a one hour period. In this example, referring to either Figure 1.1 or 1.2, but

www.manaraa.com

especially Figure 1.2, the irradiance measured at one location (top plot) is quite variable. When the irradiance is measured at 25 locations within a few hundred yards of the first sensor (middle plot), it is observed that the clouds affect each sensor at a different time. Finally, if these 25 sensors are averaged together, the bottom plots show that the average irradiance would be less variable than the single sensor irradiance.

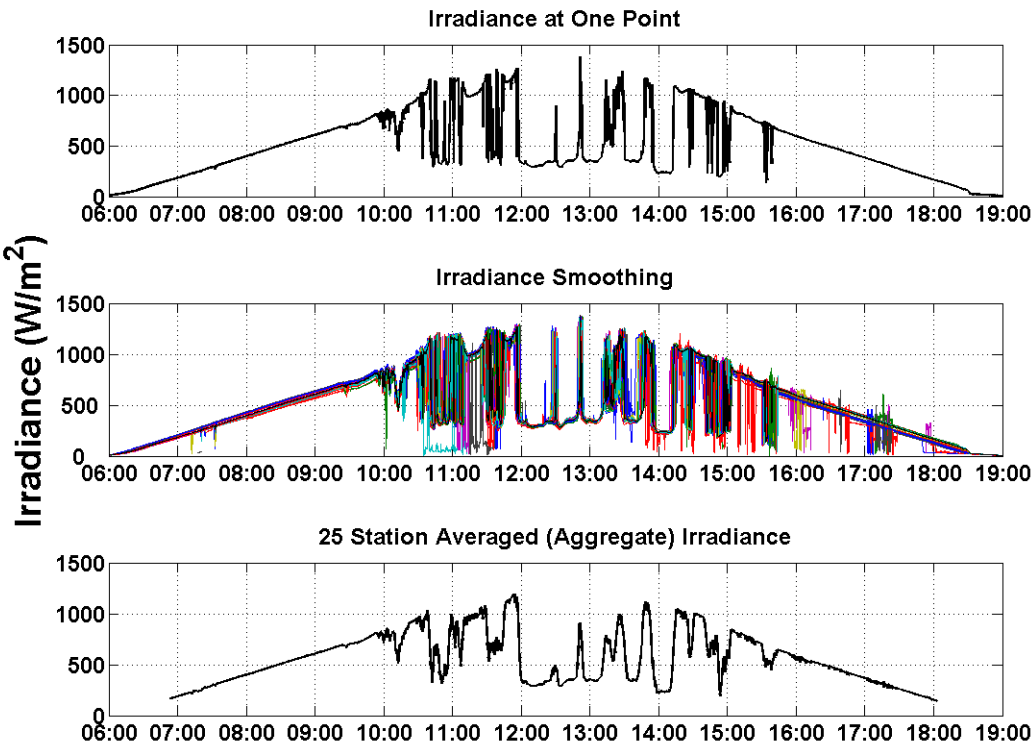

Figure 1.1: The spatial smoothing on April 12, 2013 is considered by comparing the single irradiance sensor measurement (top plot) to measurements at 25 sensors (middle), and to a smoothed irradiance signal (bottom) which accounts for the aggregated irradiance over the size of a PV power plant.

www.manaraa.com

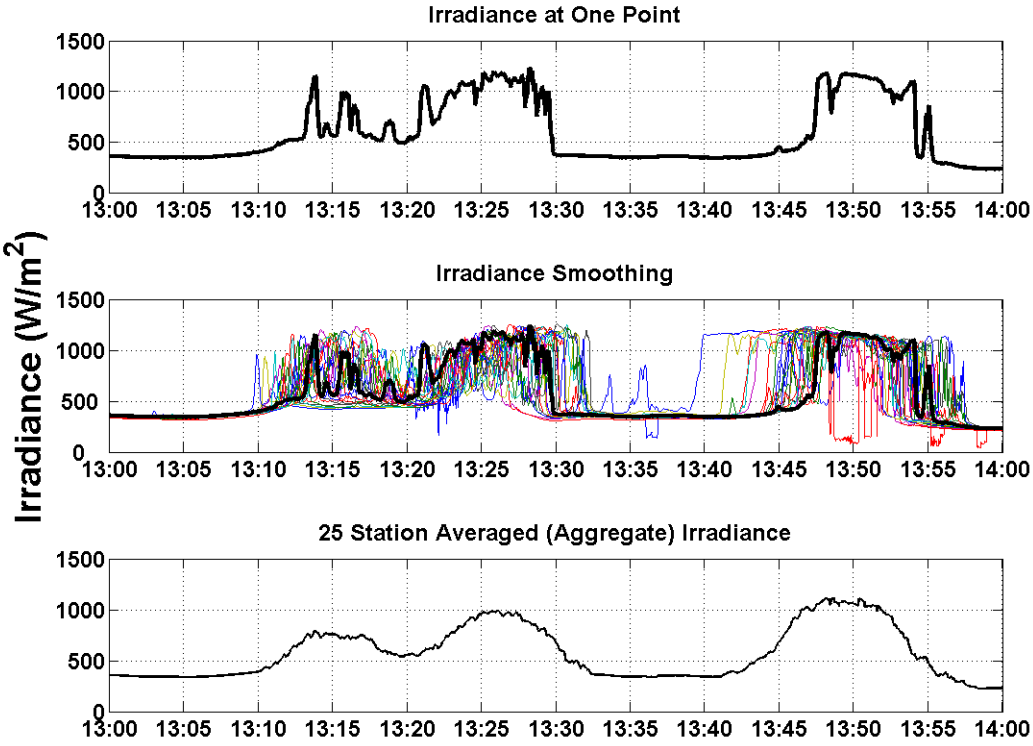

Figure 1.2: The irradiance over one hour on April 12, 2013 shows how spatial smoothing occurs over the area of a PV power plant on sub-hourly timescales.

Because solar PV generation is rapidly increasing in capacity and will soon be a significant contributor, and due to the potentially negative impact of large fluctuations in PV power, it is important to understand the spatial smoothing of solar PV power plants. The ability to predict the spatial smoothing of irradiance allows for improved planning for the integration and interconnection effects of using the variable solar PV plants. The focus of this work is to study the spatial smoothing that occurs and determine how to most efficiently deploy solar irradiance sensors to accurately predict this smoothing.

www.manaraa.com

1.2 Project background

This work utilizes data from a network of 45 solar irradiance sensors which was deployed as part of a wind and solar variability study for NextEra Energy Resources, LLC. The goal of that study was to quantify the solar and wind variabilities at a location north of Flagstaff, AZ. The solar sensors were industry standard LI-COR type 200S irradiance sensors and measured total solar irradiance on a horizontal surface in W/m^2. They were dispersed over an approximately one square mile grid and collected data every one second over an 18 month period (although data is not continuous through that time period).

1.3 Research questions

Three primary research questions are the focus of this work:

1. What is the smoothing of the irradiance profile measured from a single point irradiance sensor extrapolated to the integrated irradiance over the area of a solar PV power plant of distribution scale (1-20 MW capacity) and of transmission scale (20-40 MW capacity)?

2. How many irradiance sensors are required to predict the smoothing of distribution scale and transmission scale power plants using wavelet-based variability analysis? What is the ideal layout of those sensors?

3. What temporal sampling rate is required to capture the variability of distribution scale and transmission scale power plants?

www.manaraa.com

Chapter 2

Theory and literature review

As discussed in Section 1.1, the increase in solar PV power utilized on the electricity grid makes it important to understand the variable nature of solar PV power. This Chapter discusses variability, examines the grid impacts of variability, explores tools available for spatial smoothing and variability analysis, summarizes wavelet theory, and presents the Wavelet Variability Model.

2.1 Variability and variable generation

Variability is generally defined as "The quality, state, or degree of being variable or changeable". There are many metrics which are useful to quantify variability, but no single accepted metric to universally define the the term. The simplest metric for variability might be the standard deviation of a time series of values. A high standard deviation indicates that the values in a dataset are "far away" from the mean value, while a low standard deviation indicates that values tend to be "close to" the mean value of the dataset. In this thesis, variability is used in some discussions as a general term without referring to any specific metric, and then a few chosen variability metrics are selected and used in the analysis (see Section 2.3).

www.manaraa.com

As discussed in Chapter 1, variable generation sources (wind, solar, etc.) are distinguished from non-variable generation (coal, nuclear, etc.) because their power output varies with the available wind or solar resource, instead of being controllable by the system operator.

2.2 Grid integration and interconnection impacts of solar PV

The variability of solar PV can have an impact on the electricity grid. This impact occurs differently at the distribution system level than at the transmission system level.

Transmission and distribution systems

For the purposes of this work, it is important to distinguish between the transmission system and the distribution system on the electricity grid. The largest scale of the electricity grid is the transmission system. This system connects large generators and large loads on high voltage lines (>110 kV). The transmission system feeds into the distribution system which connects individual loads or groups of loads at low voltage (<100 kV). This distribution system can also include smaller power plants including smaller solar or wind power plants. These distribution-size plants are roughly less than 20 MW capacity. The transmission system is balanced by matching total load to available generation and maintaining system frequency and voltage. A primary job of the distribution system is to maintain system voltage.

www.manaraa.com

Impact of variability on the transmission grid

System balance on the transmission grid is maintained by matching load with generation. On grids with variable generation, the balancing is actually between net load and generation, where net load is defined as load minus variable generation. This is because changes in variable generator output are seen by the remaining dispatchable generators on the grid just the same as changes in load are seen. For example, a ramp up in solar PV power generation impacts the system the same as a ramp down in load requirements would.

The changes in load requirements are largely met by responding to those changes by controlling the output of conventional generators. The control of these generators is done on several time scales:

1. **Unit-commitment** and **scheduling** are planning for the generators that will be online based on expectations for electricity load and generation several hours to several days ahead of time.

2. **Load following** is the control of generator output based on forecasts for load or net load several minutes to hours ahead of time. Load following ensures that sufficiently flexible generation is on-line in order to track the net load expected over that timescale.

3. **Regulation** is automated control of the generators that are already online and responsive to fluctuations in net load on a short timescale (seconds ahead to a few minutes ahead).

Handling all of these transmission system considerations is referred to as "ancillary services" and determining how these services are influenced by variable generation is

www.manaraa.com

a key topic in the integration of variable generation.

Impact of PV variability on the distribution grid

When PV power plants are connected at a distribution-system level instead of at a transmission level, fast changes in the output that would be completely absorbed into the transmission system can impact the distribution system voltage. For this reason, "sub-regulation" changes are sometimes parsed out of the regulation changes. Sub-regulation changes are sub-minute changes that are handled not at the generator but on the distribution line. The handling of these distribution-system voltage changes is an important issue that must be handled during the interconnection of variable generation. Voltage balancing, whether due to variable generation or due to load fluctuations, is handled using tap changers on transformers, capacitor banks, and voltage regulation capabilities within the PV plants themselves.

If the net load is significantly more variable after the addition of new variable generators, the system must be prepared and physically capable of responding to this variability. For this reason it is important to understand the variability of these generators on all of the timescales mentioned above.

2.3 Tools for solar variability analysis

Many metrics for variability analysis exist. This sections summarizes some of the most common metrics with a focus on those metrics that are used in this thesis.

www.manaraa.com

2.3.1 Deltas and standard deviation

The simplest tools for quantifying variability are "deltas" and standard deviation of deltas. Deltas are simply the changes between subsequent irradiance (or power) values in a time series. Deltas can be considered at multiple timescales by taking different time averages of the irradiance signals and then considering the changes between subsequent averaged points. Alternatively, deltas can be determined by sampling datapoints less frequency, e.g. one might only use every 10th data point in a one-second time series to simulate lower frequency data. The standard deviation of the deltas can also be used as a variability metric [6].

2.3.2 Clearness index

The clearness index k_t quantifies the clearness of the sky by the ratio of the instantaneous irradiance to the extraterrestrial irradiance [7]. The clearness index can also be considered over periods of time such as over an hourly, daily, or annual period. In this case it is the ratio of the integrated measured irradiance to the integrated extraterrestrial irradiance over that period of time.

2.3.3 Clear sky model

A clear sky model is a model used to represent the irradiance available on the ground at a given time and location under cloudless sky conditions. Figure 2.1 provides an example of a modeled clear sky irradiance over one day compared to the actual measured irradiance.

www.manaraa.com

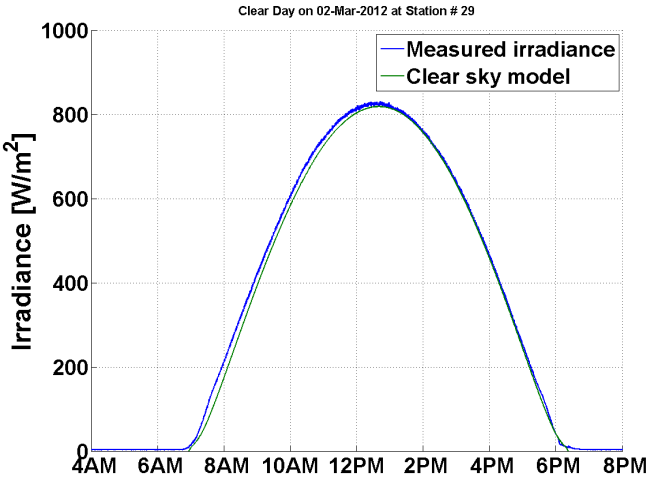

Figure 2.1: The measured irradiance on a clear day is compared to the modeled clear sky irradiance; the two signals are very similar.

Many clear sky models have been developed with various degrees of complexity. Studies have compared the different clear sky models for accuracy ([8], [9]). The general conclusion is that the choice of a clear sky model depends on the available information (inputs) for the model. Simple models exist which require only location and time data, while more complex models use elevation, air turbidity, atmospheric absorption, etc. If such detailed input data is available and reliable, it can make for a clear sky model which more closely represents actual measured clear sky conditions. In Section 4.1.1, the selection of a model for this study is discussed in detail.

2.3.4 Clear sky index

A clear sky index is used to normalize the irradiance measurements to the clear sky model to remove the solar position dependent portion of the irradiance from a dataset, and focus on the stochastic cloud movement component of the signal. A clear sky

www.manaraa.com

index is simply the measured irradiance divided by the clear sky model irradiance. A clear sky index is not only useful in separating the stochastic cloud movement component from the deterministic solar position component of irradiance, but it also is useful in comparing irradiance measurements from different locations or times of the year. One downside to the clear sky index is that it tends to give very high index values near sunrise and sunset. These values can be unrealistic because the precision of the irradiance measurements at low irradiance is poor, so a few W/m^2 difference between measured irradiance and clear sky irradiance could indicate a clear sky index much greater than one. In addition, the actual changes in irradiance on a percentage basis are high near sunrise and sunset, so to some extent these high values can also be correct.

2.3.5 Variability Index

The Variability Index (VI) is an irradiance variability metric developed by Stein, Hansen, and Reno [10]. This metric measures the variability of the irradiance by considering the length of the irradiance line. The ratio of relevance is the length of the measured irradiance line (plotted in W/m^2 vs time) divided by the length of the clear sky irradiance line. The calculation is provided in Equation 2.1, where k is the data point, n is the number of available points in a daily irradiance time series, GHI is the global horizontal irradiance, and CSI is the clear sky irradiance.

$$VI = \frac{\sum_{k=2}^{n} \sqrt{\left(GHI_k - GHI_{k-1}\right)^2 + \Delta t^2}}{\sum_{k=2}^{n} \sqrt{\left(CSI_k - CSI_{k-1}\right)^2 + \Delta t^2}} \tag{2.1}$$

On a clear day, the measured irradiance should theoretically be exactly the same

www.manaraa.com

as the length of the irradiance line, so that the VI is equal to one. On a day with many clouds passing over the irradiance sensors, the VI value will be much greater than one because the irradiance line will be fluctuating up and down with the increases and decreases in irradiance due to passing clouds. It is also possible to measure a VI value of less than one on an overcast day when the irradiance may be at a constant, low level, never increasing to the peak values predicted by the clear sky model. The ratio value can be calculated at any timescale, down to the timescale where measurements are available. To obtain the day's VI value, the VI is calculated as the sum of the measured irradiance line lengths to the sum of the clear sky model line lengths. As with any variability metric, the metric is affected by the timescale of measurement. If the VI is calculated based on one second data, it will be considerably higher than if calculated based on one minute averages of the one second data or based on raw one minute data. The authors of the VI note that this is due partially to the smoothing out of any measurement error in the measured irradiance values, and partially due to 'hiding' of the real high-frequency variability that exists under one minute. VI values range from less than one up to twenty or more, thus giving a nice range of numbers to compare daily VI values.

2.3.6 Irradiance ramps

Grid operators and system planners are interested in the ramps that the system must respond to in order to maintain balance of frequency and/or voltage. A 'ramp event' is an increase or decrease in net load at the system level, or at the generator level, an increase or decrease in power. In a solar PV variability study such as this one, it is of interest to identify the irradiance ramps and provide some quantification

www.manaraa.com

of their size and frequency of occurrence. These irradiance ramps are then useful in understanding the possible power ramps of a PV plant. These metrics are then another way of looking at the variability of the resource. The specific metrics of interest are the ramp magnitude (size in W/m^2) of the change in the power value, the ramp duration which is the length of time required for the change to occur, and the ramp rate (in $\frac{W}{m^2 t}$) which is the rate of change of the increase or decrease in power.

There is no single definition of a ramp event, perhaps because there are multiple balancing authorities and independent system operators in the U.S. which operate their systems with unique procedures and at different timescales. For this reason many variable generation studies have used different ramp definitions. For the purpose of this work, a ramp detection algorithm is implemented using the deadband method which detects ramps of different durations [11], [12]. For a discussion of the algorithm implemented, see Section 4.1. Figure 2.2 provides an example of a the ramps detected in irradiance measured over one day.

www.manaraa.com

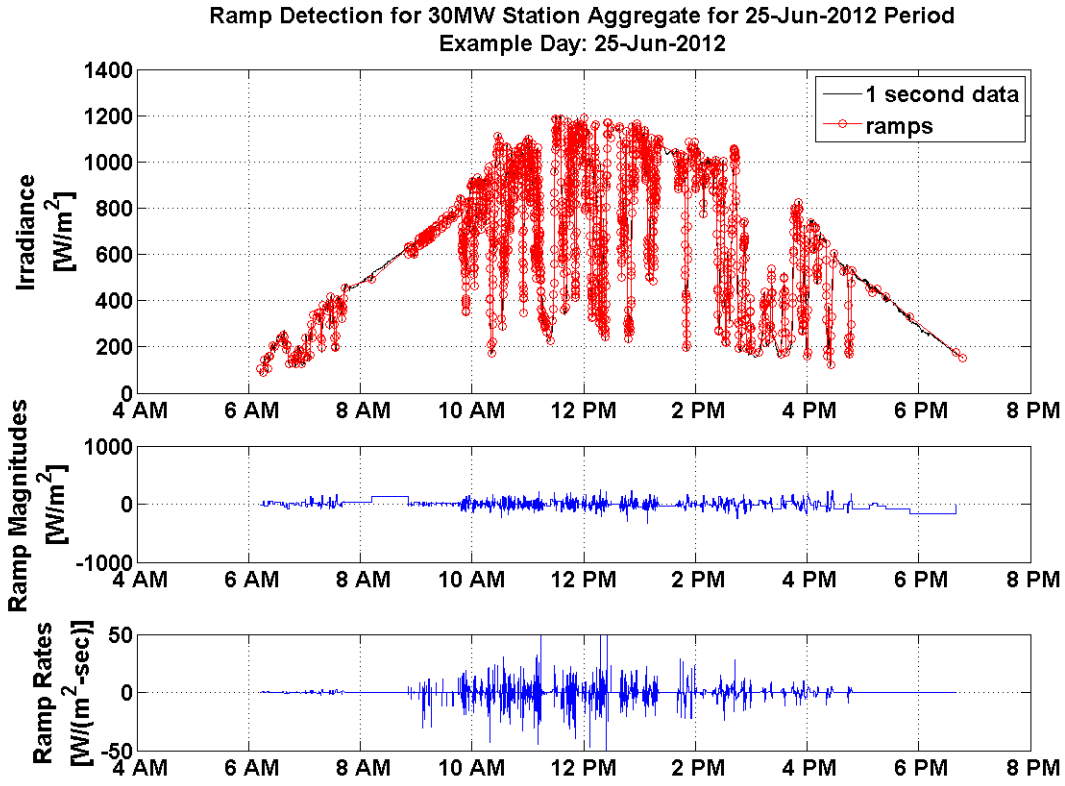

Figure 2.2: The irradiance ramps detected in a one-second irradiance signal on a highly variable day are shown in red (top plot). The magnitudes of the ramps detected are relatively small (middle), but the ramp rates of the very short duration ramps that occur on this day are high (bottom).

Once a ramp event is defined and an algorithm is selected, the variability is commonly quantified by looking at the most extreme ramp rates (95th percentile, 99.7th percentile, etc.). It is also common to look a the cumulative distribution function of the ramp rates ([13]).

www.manaraa.com

2.3.7 Daily Aggregate Ramp Rate

van Haaren, Morjaria, and Fthenakis [13] created the Daily Aggregate Ramp Rate (DARR) as a way to characterize the variability of irradiance per day. This metric is the sum of all of the absolute values of irradiance changes measured at each of the 1,440 minutes (t) throughout the day. It is assumed to be based on one minute data. The DARR calculation is:

$$DARR_{min} = \sum_{t=1}^{1440} \frac{I_t - I_{t-1}}{C} \tag{2.2}$$

Here I is the plane-of-array irradiance and C is a constant equal to 1000 W/m^2. The authors categorize the daily variability by DARR into five different categories. The least variable category is DARR less than than three, and the most variable is DARR up to 33. A perfectly clear day would have a DARR of two.

2.4 Spatial smoothing of irradiance fluctuations

As discussed in Section 1.1, smoothing of the short-term variability of irradiance over the area of a PV plant is the focus of this work. This variability occurs on the regulation, sub-regulation and load following timescales. Cloud motion over a single irradiance sensor can show large changes in irradiance on a second-to-second basis, as displayed in Figure 1.2.

2.4.1 Modeling spatial smoothing

Predicting spatial smoothing of PV power plants has been an area of recent research interest. The following is a sampling of the methods that have been used, beginning

www.manaraa.com

with the simplest:

1. Longhetto, Elisei, and Giraud [14] provided one of the earliest methods for estimation of spatial smoothing. They proposed that smoothed irradiance can be estimated by a moving average of the irradiance profile. The time interval of the moving average is determined by the length of time required for a cloud to pass over the PV plant's area. This depends on the size of the PV plant and the cloud speed. Stein, Ellis, and Hansen [15] used this method and found averaging intervals typically fell in the range of two to five minutes for a variety of plant sizes ranging 5 to 300 MW.

2. Multiple sensors can be deployed and averaged to estimate smoothing. However, deploying many sensors is costly. Several studies have been completed which use irradiance sensor networks or networks of PV power plants to quantify the intra-site aggregation effects [16], [17], [18], [19]. However, only a few studies using a dense network of irradiance sensors to capture inter-plant irradiance smoothing exist. Kuszamaul, Ellis, Stein, and Johnson [20] used a network of 16 irradiance sensors over a 1.2 MW PV power plant in Lanai, Hawaii. The sensors monitored irradiance at one second intervals. The results showed that although one sensor is a poor predictor of power, the average of all 16 sensors could be a reasonably good predictor because there was a nearly linear relationship between average irradiance and actual power output. van Haaren, Morjaria, and Fthenakis [13] used five sensors over a 48 MW PV power plant. They showed that the normalized average irradiance from the five sensors was a much better predictor of normalized power output than the normalized irradiance from one sensor. Hoff and Perez [5] cite a network of 25 sensors over a 400 m

www.manaraa.com

by 400 m grid in Cordelia Junction, CA. They use this network to study the relationship between site correlations, distance between sites, and irradiance averaging intervals.

3. Marcos, Marroyo, Lorenzo, Alvira, and Izco [21] showed that the irradiance to power conversion of a solar PV plant can be modeled as a low-pass filter. Using a fast Fourier transform of point irradiance, this method filters out high frequency (short timescale) changes in irradiance before converting the remaining components of irradiance to power. The cutoff frequency - the frequency above which fluctuations are removed from the smoothed output - depends on the power plant size.

4. Hoff and Perez [5] predicted the relative output variability of a PV power plant (variability of entire plant divided by variability of single point irradiance) using a dispersion factor (number of time intervals for a cloud to pass over a PV power plant).

5. Lave, Kleissl, and Stein [1] developed a wavelet variability model (WVM) which uses a wavelet transform to quantify the smoothing effect over a PV power plant or distributed network of small PV systems. A wavelet transform is a method of transforming a signal into sub-signals which are fit to a chosen waveform at different time scales (for details, see Section 2.6.1). The WVM uses a single irradiance sensor to model the variability of a power plant using a correlation scaling coefficient that depends on the site location and the weather conditions. The WVM has been shown to be accurate for both distributed PV applications and central PV plants [22]. It shows promise to meet the needs of modelers

www.manaraa.com

because of its accuracy and limited input requirements (solar irradiance and correlation scaling coefficient).

2.5 Spatial and temporal sampling of irradiance measurements

A few studies are available which discuss temporal sampling rates for irradiance used to determine solar PV power output. Notably, the following two studies consider the impacts of temporal sampling on a single PV module, and do not discuss temporal sampling as it relates to spatial smoothing over the area of a large PV power plant.

1. Hansen, Stein, and Riley [23] considered the effects of time-averaged weather data on modeled PV power and energy. They found that calculating power using averaged weather variables overestimates power, and that the power calculated from averaged weather data is less variable than that calculated from raw weather data. In this study the lowest temporal sampling rate of measured weather data was about three seconds, and they considered time averages of up to one hour. The array that was modeled was a 230 W solar PV array. Their recommendation was that in order to have an accurate estimate of the distribution of power, weather measurements (i.e. irradiance) have a time interval of five minutes or less. They also note that the appropriate sampling interval may be different depending on the ultimate objectives of the work. Similarly, they found that longer temporal sampling rates for input weather data result in larger errors in total energy production estimates.

2. Riley, Cameron, Jacob, Granata, and Galbraith [24] considered the effects of the

www.manaraa.com

irradiance temporal sampling rate on the modeled PV power. They compared the power determined from three second measured data to power determined from data sampled at intervals from ten seconds to one hour, and also to power determined from data sampled every three seconds and averaged over ten seconds to one hour. Their findings show that error increases with increasing interval and that error is larger when averaging over the sampling interval is not done. They also consider the effects of variability and they find that the most variable days have the largest error in power estimates. This analysis was focused on power modeled for a 215 W mono crystalline silicon panel.

Literature exploring spatial sampling of irradiance for solar PV power is rare. Kuszamaul et al. ([20], discussed above) briefly mention the need for future work which might consider the benefits of adding more sensors (their network was 16 sensors) compared to the detriments of added cost and data management. This lack of literature discussing spatial sampling is simply because few dense irradiance networks exist, and even fewer have been used to study spatial smoothing.

2.6 Wavelets and wavelet-based analysis

In this section wavelets and wavelet transforms are defined followed by a discussion of wavelet-based analysis, with particular focus on the Wavelet Variability Model.

2.6.1 Wavelets and other time series analysis tools

A wavelet transform is a transformation of a signal into sub-signals, each associated with different timescale, such that the sub-signals represent the changes in the signal

www.manaraa.com

at those different timescales. In this section the concept of a wavelet transform is discussed and compared to the better known Fourier transform.

Wavelet Transform

It is important to first note that the use of a wavelet transform in signal processing and time series analysis is a field of study in itself. The discussion in this section is provided to give a general understanding of wavelets and the WVM. It is worth noting also that the use of wavelet analysis in the WVM and the other wavelet-based analysis tools discussed in this section may differ from (and, certainly, expand on) the basic theory provided herein. The following explanation is based on Percival and Walden's textbook on wavelet methods [25].

First, a wavelet is defined. In casual terms, a wavelet is a finite in time, symmetric, normalized waveform. Mathematically there are two basic requirements for a wavelet:

$$\int_{-\infty}^{\infty} \Psi(T)dT = 0 \tag{2.3}$$

$$\int_{-\infty}^{\infty} \Psi^2(T)dT = 1 \tag{2.4}$$

These require, respectively, that the wavelet has an average value of zero and that it is normalized. Therefore a wavelet can be any number of functions (Ψ) that meet these requirements. The wavelet used in a specific analysis is chosen based on the basic signal characteristics and the desired output of the analysis. Three examples of wavelets are provided in Figures 2.3a to 2.4b.

www.manaraa.com

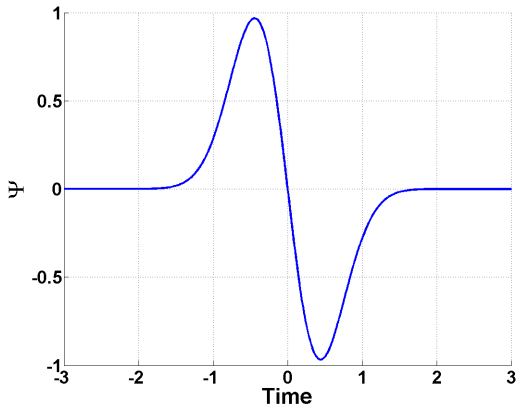

(a) Example 1 of Wavelet

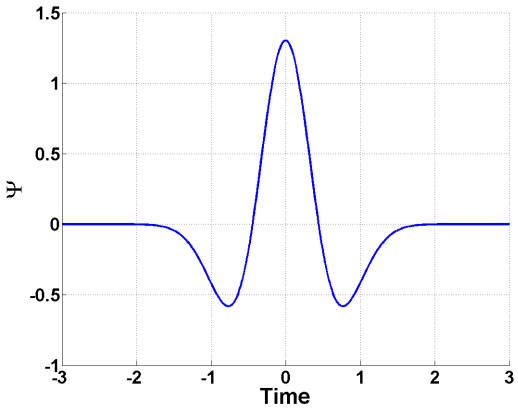

(b) Mexican Hat

Figure 2.3: These are two examples of wavelets.

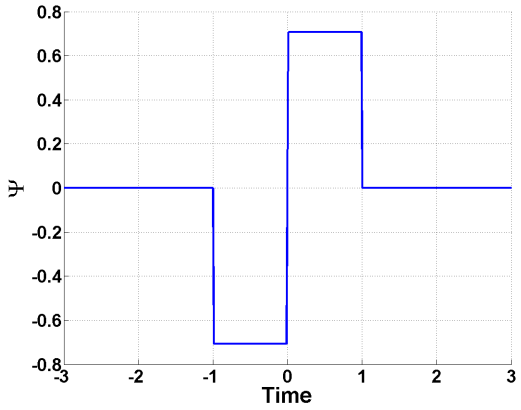

(a) Haar

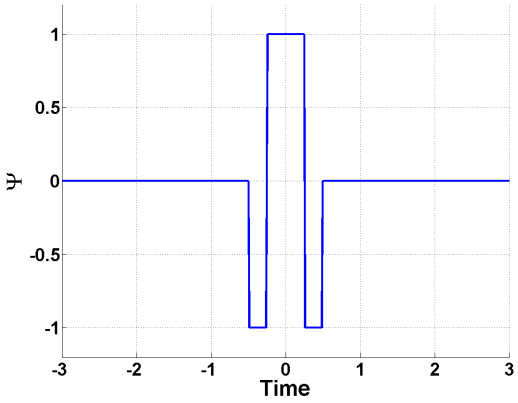

(b) Top Hat

Figure 2.4: The Haar and Top Hat wavelets are two wavelets commonly used in wavelet analysis of normalized solar irradiance signals because of their bimodal shapes.

This discussion will focus on the Haar wavelet because it and the Top Hat wavelet, another step-function type wavelet, are typically used in solar analysis because of the bimodal behavior of a clear sky index time series. The Haar wavelet is defined by:

www.manaraa.com

$$\Psi(T) = \begin{cases} -\frac{1}{\sqrt{2}} & : -1 < T \leq 0 \\ \frac{1}{\sqrt{2}} & : 0 < T \leq 1 \\ 0 & : else \end{cases} \tag{2.5}$$

Wavelets transformations tell us how much the weighted averages change from one period to the next. In the case of the simple Haar wavelet, weighted averages are not detected, just simple averages. To link wavelets to weighted averages, we begin with considering how an average is calculated. The average A of a function $k(T)$ over a time interval λ around time t is:

$$A(\lambda, t) = \frac{1}{\lambda} \int_{t-\frac{\lambda}{2}}^{t+\frac{\lambda}{2}} k(T)dT \tag{2.6}$$

And the difference D in the average from one time step before t to one time step after t is:

$$D(\lambda, t) = A\left(\lambda, t + \frac{\lambda}{2}\right) - A\left(\lambda, t - \frac{\lambda}{2}\right) = \frac{1}{\lambda} \int_{t}^{t+\lambda} k(T)dT - \frac{1}{\lambda} \int_{t}^{t-\lambda} k(T)dT \tag{2.7}$$

The two integrals that make up the difference D can be written as one integral using a step function $\beta(T)$.

$$\beta(T) = \begin{cases} -\frac{1}{\lambda} & : t - \lambda < T \leq t \\ \frac{1}{\lambda} & : t < T < t + \lambda \\ 0 & : else \end{cases} \tag{2.8}$$

www.manaraa.com

$$D(\lambda, t) = \int_{-\infty}^{\infty} \beta(T)k(T)dT \tag{2.9}$$

This function β resembles the Haar wavelet. If differs by the factor of $\frac{\sqrt{2}}{\lambda}$ and instead of being centered at zero and having non zero values over the interval of width 2, it is centered at time T and has non zero values over the interval $2\sqrt{\lambda}$. Therefore the integral of the product of the Haar wavelet Ψ and the function $k(T)$ will provide something that is proportional to the difference D, which represents the difference in average values between two consecutive periods in time. Adding a scale of $\frac{1}{\sqrt{\lambda}}$ to the Haar wavelet will mean that it is still normalized and the resulting wavelet transform for different timescales λ will have comparable magnitudes. Therefore the Haar wavelet for any timescale (λ) is:

$$\Psi(T) = \begin{cases} -\frac{1}{\sqrt{2\lambda}} & : t - \lambda < T \leq t \\ \frac{1}{\sqrt{2\lambda}} & : t < T \leq t + \lambda \\ 0 & : else \end{cases} \tag{2.10}$$

The integral of the product of this normalized Haar wavelet and the function is called $W^H(T)$ for a particular timescale. If this is executed for all possible timescales λ, we obtain the continuous wavelet transform $W^H(\lambda, t)$:

$$W^H(\lambda, t) = \int_{-\infty}^{\infty} \Psi(T)k(T)dT \tag{2.11}$$

The meaning of W^H at any particular point is that it is proportional to the difference between two adjacent average values of scale λ before and after time t. So, in solar variability, if the irradiance is at first steady and then quickly spikes up for

www.manaraa.com

three seconds, this would not be captured in a timescale of one minute. But on a timescale of four seconds, W^H would indicate that the four second average before that point is much different than the four second average after that point.

The discussion above considered a simple, continuous wavelet transform using the Haar wavelet. Use of a continuous wavelet transform like this provides a great deal of data. In using a wavelet transform for real applications, a discrete version is more practical. The discrete wavelet transform (DWT) implements the transform on dyatic timescales (i.e. 2^{j-1} seconds). The transform is then completed at timescales of 2, 4 and 8 seconds continuing up to the maximum timescale of interest for the application. Not only is the timescale (λ) limited to these values, but also the evaluations of the transform are not done at every timestep available. Instead, the evaluation is completed at a representative number of samples depending on the timescale. At a timescale of λ=2 seconds, for example, the evaluation is done every four seconds. For a longer timescales of λ=128 seconds, the evaluation is completed every 256 seconds. Figure 2.5 shows an example of the discrete wavelet transform of an irradiance time series. The top plot on the figure shows the raw, normalized irradiance timesignal (clear sky index) in black. Going down the figure, each plot shows a series of wavelet coefficients at increasingly smaller timescales. The pink lines indicate smoothed irradiance which is not relevant for this discussion.

www.manaraa.com

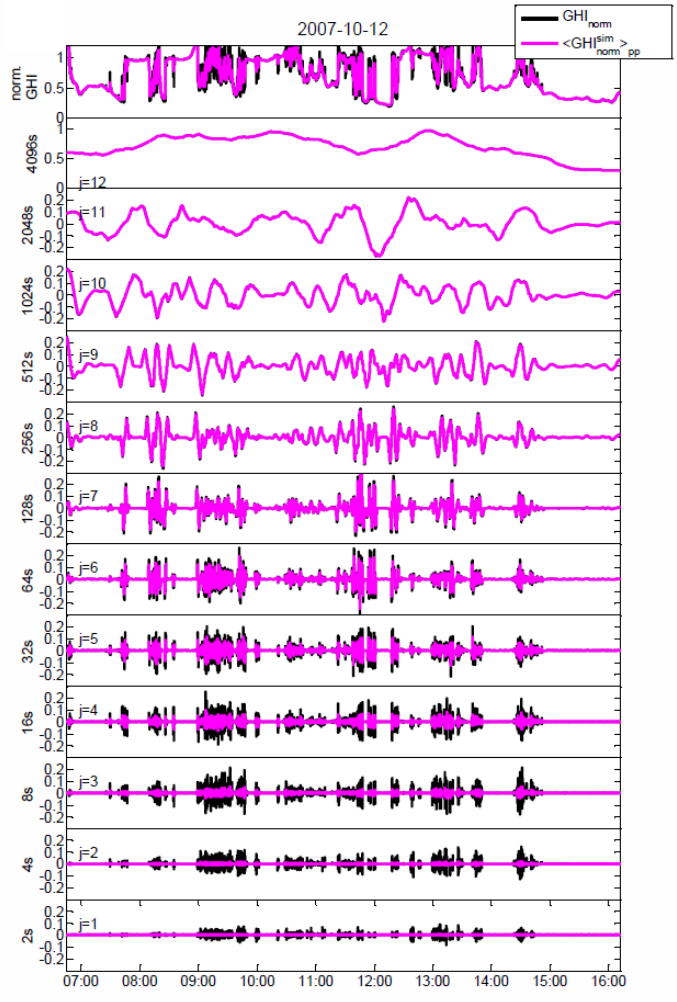

Figure 2.5: An example of a discrete wavelet transform on a normalized irradiance signal [1] showing the resulting wavelet coefficients at each timescale.

More commonly, the results of a wavelet transform are considered using a periodogram. The terms in the periodogram (I^H) are determined via:

$$I^H(\lambda, t) = \frac{1}{\sqrt{\lambda}} \left(W^H(\lambda, t)\right)^2 \tag{2.12}$$

All of the periodogram values will then be positive. An example of a periodogram

www.manaraa.com

from an irradiance transform using the Haar wavelet is shown in Figure 2.6.

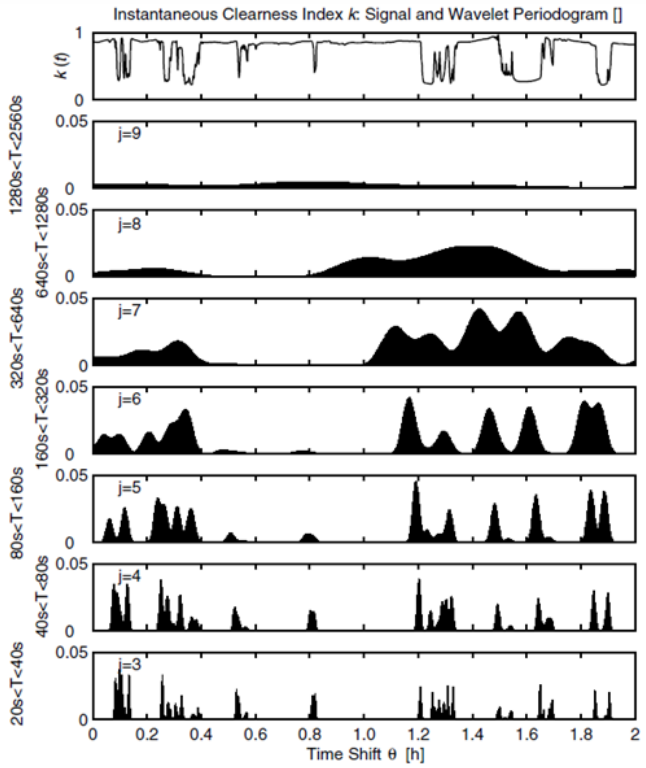

Figure 2.6: An example of wavelet transform periodogram [27] for a wavelet transform of a clearness index time series.

Comparison to Fourier Transform

A Fourier transform can also be used to analyze solar irradiance data. The two tools, however, do not provide identical results. Both methods provide information about persistence (timescale) of fluctuations. But the Fourier transform provides information in the frequency domain, while the wavelet transform captures information in the time domain. That is, the wavelet transform detects when fluctuations occur in time. These things can also be accomplished with one of the many Fourier transform models that exist such as a windowed Fourier transform. But the wavelet transform

www.manaraa.com

is relatively fast compared to the Fourier transform, and so, being able to accomplish these tasks, is preferred in some applications. Other benefits of using a wavelet transform for irradiance analysis is that base wavelets (such as the Haar wavelet) can be chosen which have similar bimodal behaviours to the clear sky index.

2.6.2 Wavelet-based analysis

Wavelets have been used for solar irradiance analysis in the literature over the last few decades. This section summarizes those applications. Discussion of the Wavelet Variability Model is in Section 2.7.

Kawasaki, Oozeki, Otani, and Kurokawa: Frequency analysis to determine average spectrum

This research [26] uses both a Fourier Transform and Wavelet Transform of one minute irradiance data collected on a 4x4 km grid of 9 stations. It is proposed that use of both transforms is optimal since the Fourier transform will provide frequency information (fluctuation) over each day, while the wavelet will provide the magnitude of fluctuation for specific time periods and for specific frequencies. The main focus of this work was to model the smoothing effect.

As a measure of the fluctuations in the frequency band of most concern, they used average spectrum which was determined as an average of the power spectrums over $1x10^{-3}$ Hz (about 15 minutes) in a given day. This was determined through Fourier analysis. As a measure of the magnitude of the fluctuations on the timescales of concern, a magnitude of fluctuation [W/m^2] was calculated based on the wavelet analysis. The magnitude of fluctuation is calculated by determining the maximum

www.manaraa.com

spectrum from wavelet analysis and multiplying that maximum value by the time period. For variable days, it was seen that both the magnitude of fluctuation and the average spectrum were decreased at the average of the 9 sites compared to any individual sensor.

Woyte, Belmans, and Nijs: Definition of fluctuation power index, characteristic persistence, and fluctation energy index

This work [27] focuses on the use of localized spectral analysis via wavelet analysis to examine fluctuations in clearness index due to cloud movement. Wavelet analysis was based on the Haar wavelet due to its similarity to the bimodal behavior of the clearness index. Three terms are introduced: fluctuation power index (cp_f), characteristic persistence (T_j), and fluctuation energy index (cf_e). Fluctuation power index at a specific time scale (2^j in wavelet analysis) quantifies the duration and severity of power changes. Characteristic persistence at a specific time scale (2^j) is the typical length (persistence) of a cloud-induced irradiance state. At any time scale, multiplication of the fluctuation power index by the characteristic persistence gives the fluctuation energy index which is useful in planning for energy storage or demand side management techniques to compensate for the solar variability.

For solar irradiance at several sites measured at one to five second resolution, the relationship between cp_f and T_j was analyzed. A daily clearness index (k) was used to quantify the sky conditions. This allows the cp_f and T_j relationship to be looked at by the type of sky conditions for that day and it was found that for the sites examined, there is a characterstic relationship cp_f and T_j depending on k.

www.manaraa.com

Lave, Kleissl, and Araias-Castro: Application of fluctation power index, use of wavelet decomposition to quantify smoothing

Analysis of solar variability via ramp rate analysis as well as analysis of geographic smoothing via wavelet analysis was done [19]. The data used for this analysis was six solar resource stations at 1-second resolution. The site were all with 3km of each other. The ramp rate analysis considered ramps determined from moving averages as well as block averages. Wavelet analysis used the fluctuation power index as described above, developed by Woyte et. al., 2007. The fluctuation power index values were calculated at a number of timescales of interest for both a single sensor and the average of the six sensors. The ratio of the fpi at one site to that for the average of sites was considered a metric of variability reduction and it was found that this variability reduction was large (about 6) for timescales under four minutes, and then decreased to about one (no variability reduction) at timescales greater than one hour. A wavelet decomposition using the top hat wavelet was completed at each timescale and also for both the single sensor and the average of six sensors. This wavelet decomposition also allowed for comparisons of variabilities at each timescale, since the wavelet transform indicates changes in weighted averages. These results also indicated that variability reductions were large at short timescales under one hour, and small for timescales around an hour or more. The results were compared to the Hoff and Perez (2010) dispersion factor model and it was found that the variability reductions found at the short timescales using the wavelet decomposition were greater than those predicted using the dispersion factor model. At higher timescales they were the same.

www.manaraa.com

2.7 Wavelet Variability Model

The WVM developed by Lave, et al. [1] is the chosen tool for this work because it has been shown to accurately predict spatial smoothing and because the dataset available in this work is particularly well suited to work with the model (having a large network of irradiance sensors that can be used to obtain the necessary correlation scaling coefficient). As discussed above, the WVM uses a single point irradiance sensor and a correlation scaling coefficient to model total, smoothed irradiance over a PV power plant or a network of distributed PV sites. In short, the model uses a wavelet transform to parse the irradiance signal into sub-signals that represent irradiance changes on timescales from two seconds to 4096 seconds, then uses a constant called Variability Reduction at each timescale to smooth the sub-signal at each timescale. Finally the smoothed sub-signals are aggregated via a reverse wavelet transform to obtain a smoothed irradiance signal. This section describes the model in further detail.

2.7.1 Variability reduction

The Variability Reduction (VR) is defined as the ratio of the variance of the changes in normalized irradiance at an individual sensor to the variance of the changes in irradiance averaged over the entire power plant footprint. VR is different depending on the timescale of the irradiance measurements. Equation 2.13 is the basic definition of VR:

$$VR = \frac{\sigma^2_{onesite}}{\sigma^2_{average}} \tag{2.13}$$

www.manaraa.com

VR can also be written as a function of station pair correlations and number of sites N, where station pair correlations are the correlations of the changes in irradiance between each possible pair of stations m and n which are a distance $d_{m,n}$ apart, and where irradiance is averaged on a timescale t, $\rho(d_{m,n}, t)$.

$$VR(t) = \frac{N^2}{\Sigma_{m=1}^{N}\Sigma_{n=1}^{N}\rho\left(d_{m,n}, t\right)} \tag{2.14}$$

These two definitions are equivalent. The derivation begins with the definition of variance.

$$\sigma_{average}^2 = VAR\left(\frac{\Sigma_{i=1}^{N} GHI_{\Delta t}}{N}\right) \tag{2.15}$$

The variance of the sum is the sum of the covariance of all possible combinations.

$$VAR\left(\frac{\Sigma_{i=1}^{N} GHI_{\Delta t}}{N}\right) = \Sigma_{i=1}^{N}\Sigma_{j=1}^{N} COV\left(\frac{GHI_{\Delta t,i}}{N}, \frac{GHI_{\Delta t,i}}{N}\right) \tag{2.16}$$

From definition of covariance:

$$\Sigma_{i=1}^{N}\Sigma_{j=1}^{N} COV\left(\frac{GHI_{\Delta t,i}}{N}, \frac{GHI_{\Delta t,i}}{N}\right) = \Sigma_{i=1}^{N}\Sigma_{j=1}^{N} \frac{\sigma_{\Delta t,i}^2}{N}\frac{\sigma_{\Delta t,j}^2}{N}\rho_{\Delta t,i,j} \tag{2.17}$$

$$\Sigma_{i=1}^{N}\Sigma_{j=1}^{N} COV\left(\frac{GHI_{\Delta t,i}}{N}, \frac{GHI_{\Delta t,i}}{N}\right) = \frac{1}{N^2}\Sigma_{i=1}^{N}\Sigma_{j=1}^{N}\sigma_{\Delta t,i}^2\sigma_{\Delta t,j}^2\rho_{\Delta t,i,j} \tag{2.18}$$

Therefore from the first definition of VR,

www.manaraa.com

$$VR = \frac{N^2 \sigma^2_{onesite}}{\Sigma^N_{m=1} \Sigma^N_{n=1} \sigma^2_i \sigma^2_j \rho_{i,j}} \tag{2.19}$$

Assuming that the standard deviations of the individual sites are the same, the standard deviations come out of the summation and cancel and we get Equation 2.20. The VR can range from 1 to N. These two definitions are equivalent.

$$VR = \frac{N^2}{\Sigma^N_{m=1} \Sigma^N_{n=1} \rho \left(d_{m,n}, t \right)} \tag{2.20}$$

In the WVM, VR is determined using correlations between a dense network of theoretical irradiance measurement sites within the PV power plant. The correlation scaling coefficient is what allows measurements from the actual measurement sites to be extrapolated to these theoretical irradiance sites.

2.7.2 Correlation scaling coefficient

In order to obtain the correlations between sites which determine the VR, the WVM uses a correlation scaling coefficient, A $[m/s]$, which accounts for how station pair correlations depend on distance between stations as well as timescale of measurement. Stations which are further apart are generally less correlated on a given day, and similarly irradiance averaged over a long timescale such as an hour are more correlated on a given day. This coefficient, A, depends on the cloud speed at a given site on a given day. In order to determine A for a given day, a small network of sensors (about five) can be used, or alternatively, cloud speed estimates can be used [22]. Since in this study the irradiance measurements from 45 stations were available, the first method is used. The correlation between normalized changes in irradiance at

www.manaraa.com

site pairs (ρ) is related to the correlation scaling coefficient A, distance between pairs ($d_{m,n}$), and timescale of measurements (t) via the following relationship:

$$\rho = exp^{\left(\frac{-d_{m,n}}{At}\right)} \tag{2.21}$$

The coefficient A is determined by a best fit of the measured data for a given day to the following equation, which comes directly from the above:

$$\rho = \left(exp^{\left(\frac{-d_{m,n}}{t}\right)}\right)^{\left(\frac{1}{A}\right)} \tag{2.22}$$

From the known A coefficient, the correlations between stations in the network of theoretical irradiance measurement sites is determined using equation 2.21 or 2.22. Finally, Equation 2.20 is used to determine the VR at each timescale.

2.7.3 Wavelet Variability Model logic

After determination of the A value and VR at each timescale, a wavelet transform is employed. The measured point irradiance is normalized using a clear sky index. The WVM uses the "top hat" wavelet and defines a special definition for the wavelet transform at the highest time interval so that the sum of the wavelet transforms at all time intervals equals the original signal. The wavelet transform uses this base wavelet (top hat) and determines the wavelet coefficients shifted and scaled at each time scale. A series of these coefficients compose the sub-signals at each timescale (see black lines in Figure 2.5).

Next the variability reduction at each timescale is applied to the irradiance at each timescale by dividing the wavelet sub-signal by the square root of the variability

www.manaraa.com

reduction at that timescale according to Equation 2.13. This results in a smoothed irradiance at each timescale (see pink lines in Figure 2.5). Finally, these smoothed irradiance signals are aggregated via a reverse wavelet transform to obtain a smoothed irradiance signal over the entire power plant. An example of the single point sensor irradiance and final modeled smoothed irradiance is provided in Figure 2.7.

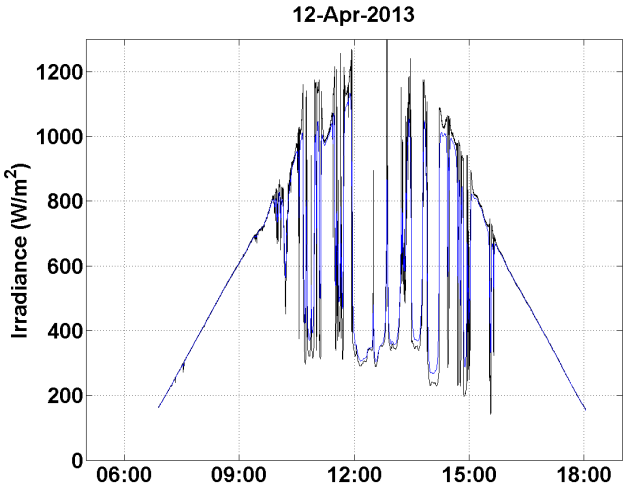

Figure 2.7: The WVM uses point sensor irradiance (black), an A-value, and the size of the PV power plant to determine spatially smoothed irradiance (blue).

Sandia National Laboratories and the University of California have made available a GUI-based version of a MATLAB program which implements the WVM. The inputs to the WVM are point irradiance, power plant location (latitude and longitude of boundaries), correlation scaling coefficient, and power plant density in W/m^2. The model outputs smoothed irradiance, variability reduction at each of 10 standard timescales from 2-seconds to 4096 seconds, and fluctuation power index which is a measure of the power content of fluctuations at each timescale, as well as the original inputs. This program is used to model the smoothing for this project.

www.manaraa.com

Chapter 3

Solar irradiance dataset: data collection and quality control

This thesis work is part of a larger wind and solar variability study with NextEra Energy Resources. The solar dataset was collected from a network of 45 irradiance sensors which were deployed for 18 months in a location 40 miles north of Flagstaff, AZ. This chapter summarizes the dataset used for the project, the data collection process, and the quality control that was implemented prior to the start of the analysis.

3.1 Description of the dataset

The 45 irradiance sensors were deployed over a one-square mile grid. Figure 3.1 shows the sensor layout. The sensors are on a 590 ft grid in the center part of the network and on a grid of up to 1,770 ft in the less dense outer parts of the network. Using this network of sensors, two different size power plants are considered in this study. A distribution scale 10 MW plant is represented by using the inner 9 stations, and a transmission scale 30 MW plant is represented using the inner 25 stations. The plant footprints were selected using a density of 0.125 MW PV capacity per acre (i.e. 8

www.manaraa.com

acres per MW). Figure 3.1 shows the plant footprints.

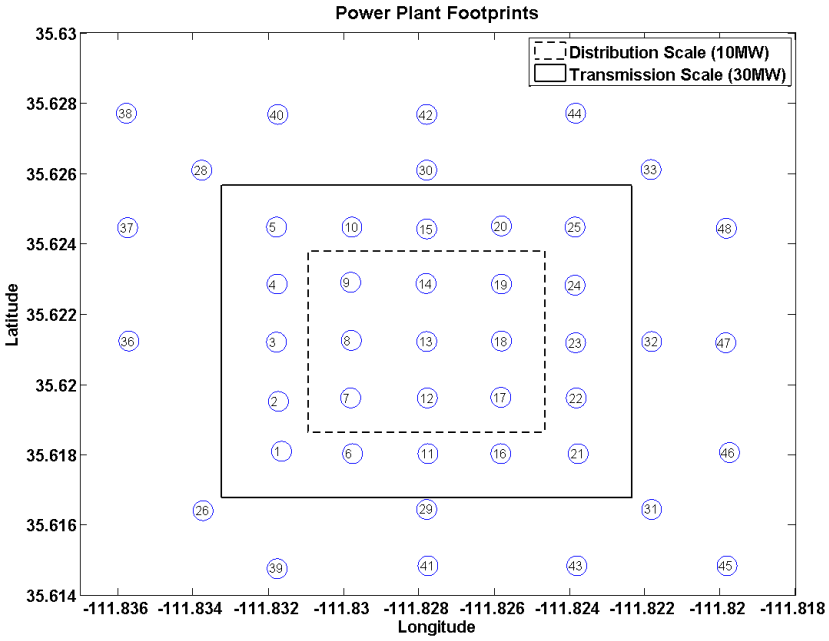

Figure 3.1: The 45 irradiance sensors used in the NextEra study were located over a one square mile grid. Two power plant sizes within that grid were examined in detail for this thesis.

The 45 LI-COR brand type 200S irradiance sensors measured global horizontal irradiance. These sensors are industry standard for this type of study due to their relatively low cost. Each sensor was mounted on a fence post along with a custom datalogger powered by a small PV panel as shown in Figure 3.2. One second data was collected including irradiance, time, chip temperature and raw voltage signal (from which irradiance is calculated). A data chip was used in the datalogger to store this one second data for up to one month.

www.manaraa.com

Figure 3.2: Each irradiance sensor used in the study was mounted on a fence post and connected to a datalogger box, which was powered by a small PV panel.

The total data collection period was from November 2011 to May 2013. Since the datalogger availability was subject to the availability of solar irradiance to charge the datalogger battery as well as temperature challenges to the batteries, the final dataset does not cover the entire period.

3.2 Summary of data collection

Data collection was completed by swapping out the data chips manually every one to four weeks. The procedures for data collection included resetting the clock, as some time drift was expected to occur between site visits. In order to maintain the integrity of the one-second data time-synced data over the array of sensors, GPS watches (or

www.manaraa.com

watches that were otherwise time-synced to standard time) were used as the basis for resetting the clocks. When the clock was reset, the amount of time drift which had occurred between that and the previous collection period was recorded. A text file from the removed chip was saved to a master folder of datafiles on campus.

3.3 Summary of quality control

A data quality control process was completed by a team of NAU graduate students and researchers at the end of the data collection period (May 2013). A short summary of each of the tasks completed is provided here:

1. The first task was to compile the over 1,000 individual text files into one master database useable in MATLAB. This task included some high level quality control which screened out bad datafiles and empty datafiles.

2. A time sync check and repair was completed for each imported text file. This included both time sync repairs based on the time sync records completed by the staff while completing onsite data collection as well as time sync repairs based on errors in timestamp detected by using the exact known sunrise and sunset times for this location and time of year.

3. After decommissioning the sensor network, the calibration of the sensors was checked in a test on campus and the sensors were found to be within their expected measurement tolerance compared to a newly calibrated sensor.

4. A correction to the irradiance was made to account for the tilt of some of the fence posts (and therefore irradiance sensors). The tilted stations were detected

www.manaraa.com

by comparing irradiance on a clear day to that predicted by a clear sky model.

5. Random, short (1-30 second) holes in the dataset due to intermittent datalogger operation were filled. One second holes were filled simply using an average of the recorded irradiance for the data points before and after the missing datapoint. Holes from 2-30 seconds long were filled using a Markov chain based technique which relies on the irradiance measured at the 4 nearest stations.

6. The data was checked for random, short (up to 30 second) drops in irradiance that were also thought to be due to intermittent datalogger operation. Where these dips in irradiance were determined to be likely due to data logger problems (not actual cloud movement), they were corrected using the Markov chain based technique.

This process improved the quality of the dataset by eliminating known problems while maintaining the integrity of the measured data.

www.manaraa.com

Chapter 4

Analysis and results

This chapter summarizes the variability metrics which were chosen, describes exactly how the Wavelet Variability Model was setup and implemented, and presents results to answer the three basic research questions.

4.1 Implementation of selected variability metrics

Of the many available metrics and measures used for studying solar variability, this study used VI analysis, irradiance ramps, regulation ramps, and sub-regulation ramps. The VI metric requires a clear sky irradiance time series. This section summarizes the specific methods used to implement a clear sky model, calculate VI, identify regulation and sub-regulation signals, and detect ramps of all three types.

4.1.1 Clear sky model

The purpose of this task was to select a clear sky model, calibrate it to this dataset, and create a time series of clear sky irradiance that covers the entire data period. The clear sky model is used not only for the VI calculations but also for the calculation of the A-value used in the WVM.

www.manaraa.com

Selection of model and goals of calibration

For this work, the methods of Reno, Hansen, and Stein [8] are closely followed. That report compares the accuracy of nine different clear sky models in predicting clear sky conditions using irradiance measured at 30 sites. The root mean square error (RMSE) and mean bias error (MBE) were used to measure the accuracy of the models. The models' accuracies were examined for different times of year, times of day, locations, elevations, and zenith angles. The results of the work show that a model called the Ineichen model achieves an overall RMSE and MBE of 0.05. This is the best overall result other than one model which requires a great deal of atmospheric measurements. The remaining models had RMSEs of just over 0.05 to up to 0.18. When looking at the model error dependence on site elevation, the Ineichen model showed little dependence on site elevation; i.e. the model performed about the same no matter what elevation the site was at.

The purpose of this work was to calibrate one of the models to represent the clear sky conditions at the site adequately, but do so in a limited amount of time so that analysis efforts could be focused on the solar variability and spatial smoothing. Although both the Ineichen model and the well-known Bird model showed similar accuracy in comparison to measured clear sky days during the initial screening, the Ineichen model was selected due to the simplicity of the model's inputs and the model's ability to account well for elevation.

Clear day selection

A set of six clear days were chosen to calibrate the model to. The days were selected to represent different times of the year. Out of the 551 days in the dataset, the available

www.manaraa.com

days were first reduced by filtering out those that did not have at least 50% of the stations individually achieving 50% uptime during the day. Although not necessary for the clear sky model, using a day with good uptime was desirable as the clear days selected for this process were expected to be used in other portions of the variability analysis which use multiple stations. Next, the remaining days were categorized by variability using the variability metric Natural Variability of Irradiance (NVI) [12]. Using this screen in combination with visual screening of the days irradiance profile (some days had a higher daily NVI average but actually appeared very clear), the six days were selected. Because of the difference in measured irradiance within the 45 stations due to calibration and station tilt angle, it was best to choose one representative station with which to calibrate the model. In order to determine which station was representative of the measured irradiance, the stations were ranked by the irradiance measured at solar noon. The median eleven stations were screened to find one station on each day that did not show any strong tilt characteristics (measurement stations that became un-level during the 18 months of use could be detected via an asymetric diurnal shape of the measured irradiance) and that had the most clear profile (no small clouds or other drops in irradiance). For all but two dates, the selected station was one of the eleven median irradiance stations. In the two cases where none of the eleven median stations were usable, another station was selected. Table 4.1 shows the clear days selected and station number which was selected for model calibration.

www.manaraa.com

Table 4.1: Six clear days from the dataset were selected for calibration of the clear sky model. On each of the six days, one station was selected to use for model calibration.

Clear Sky Date	Representative Station Selected
3/2/12	28
6/5/12	29
7/18/12	32
10/14/12	10
11/24/12	23
1/20/13	22

Ineichen model

The Ineichen model [28] inputs are time, location, elevation, and Linke Turbidity. The Linke Turbidity (TL) is the only adjustable input, so its meaning is discussed here.

TL is a measurement of the atmosphere's turbidity on a cloudless day. To understand TL one must understand optical thickness and air mass. Optical thickness is a measurement of the fraction of irradiance that is not scattered or absorbed on a path. It is a function of the clear sky beam normal radiation (B_{nc})) and the solar constant radiation (I_o). The clear sky beam normal radiation is the radiation directly from the sun's rays on a clear day, not accounting for that scattered through the atmosphere and off of the ground (both of which compose diffuse radiation). The solar constant is the radiation incident from the sun at the outside of the earth's atmosphere, which is approximately 1,367 $\mathrm{W/m^2}$. The optical thickness (δ) is:

$$\delta = -\ln \frac{B_{nc}}{I_o} \tag{4.1}$$

The optical thickness of a clear, dry atmosphere is δ_{cda} , and that of a cloudless

www.manaraa.com

atmosphere is δ_{clear}.

Air mass (AM) is the ratio of the optical path length (distance through which sunlight travels) to the optical path length when the sun is at its zenith. Many formulations for AM exist as the AM increases towards infinity at high zenith angles as the sun approaches the horizon. AM depends on zenith angle and must be corrected for lower pressure air at elevation.

TL is the number of clean and dry atmospheres that would produce the same transparency as the actual atmosphere does with the real effects of aerosols and water vapor that are in the atmosphere at a given time. It is related to optical thickness by:

$$\delta_{clear} = \delta_{cda} \times TL \times AM \tag{4.2}$$

The unique aspect of the Ineichen model is that the authors created a new formulation for TL which is more stable throughout the day than prior models.

Model calibration

Prior to model calibration against measured irradiance, some goals for calibration were set in order to account for the inherent error in the LI-COR measured irradiance, which is generally up to 5% [29]. During the calibration completed for this project, the sensors and datalogger assembly's irradiance measurements were found to be ± 2% from a reference pyranometer at high irradiance, which is equivalent to an error of ± 20 W/m^2 at 1000 W/m^2 incoming irradiance. Therefore it was expected that the clear sky model could only be calibrated up to this level of precision. A 40 W/m^2 difference could be expected between a clear sky model and measured irradiance. The goal for calibration of the clear sky model was to achieve 0.05 Root Mean Square Error

www.manaraa.com

(RMSE) and Mean Square Error (RME) because these were the best results achieved by Reno et al [8].

To implement the Ineichen model, TL can be either measured from direct beam irradiance measurements or it can be estimated using a database of values which were made determined by Remund, et al. [30]. The uncalibrated model was first done using the database values. Figure 4.1 shows those values as well as values for other southwest locations for comparison. This shows the importance of the source of the TL value; TL values vary by a factor of two for different locations.

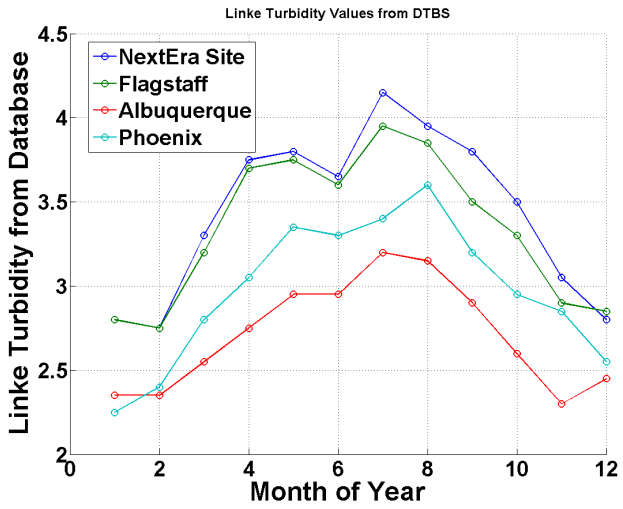

Figure 4.1: Linke Turbidity coefficients vary by time of year and location.

The first attempt to calibrate the model was focused on adjusting the database TL value. Measurements of direct beam irradiance, which were available from an RSR-2 type sensor at the project site, can be used to calculate TL values. However attempts to adjust the TL value did not improve the model's calibration and so were abandoned. Since the uncalibrated Ineichen model matched well with irradiance measured with a Kippen-Zonen thermopile type sensor at the site, and the Kippen-

www.manaraa.com

Zonen measurements were regularly 5% higher than the LI-COR measurements at this site, it was determined that a scale factor might be appropriate to calibrate the model. This scaling method is mentioned by Reno et al. as one step that may be necessary in order to calibrate a clear sky model to a specific measurement device, taking into account possible calibration issues within that device. Scaling factors of 2.5%, 5%, and 10% were tested and the results were compared. As expected, the 5% scale factor brought the modeled irradiance closest to the measured values. The average of the one-second RMSE and MBE were calculated over each of the six days. In order to determine how the average error changed as the time of day approached sunrise or sunset, the average error was calculated first including the entire 24 hour period, and then including only ten minutes before and after solar noon (labeled "solar noon" in figures), or including a certain window around solar noon (2, 3, 4, or 5 hours).

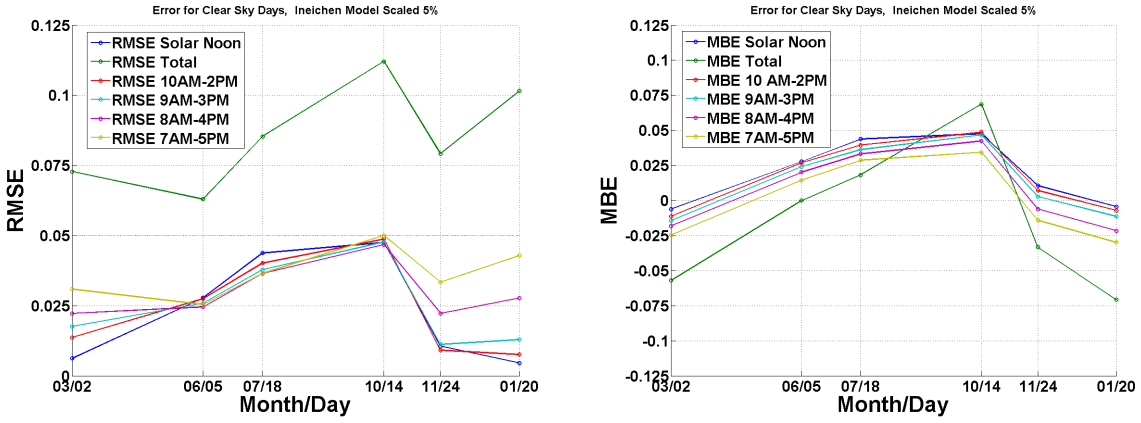

(a) RMSE (b) MBE

Figure 4.2: The error terms (RMSE and MBE) show that the clear sky model predicted well the irradiances measured on six clear sky days and for different times of the day.

www.manaraa.com

Figure 4.2a shows that although the overall RMSE is more than 0.05, this is due mostly to the overnight and early morning/late afternoon hours. When the window is shortened to only consider a 10 hour day or less, the RMSE is always less than 0.05. It is notable that on 11/24/12 and 1/20/13, the number of daylight hours was almost exactly 10 (9.87 and 9.95, respectively). This means that for these two days, the 10 hour window considered essentially every hour of daylight and the overall RMSE was still less than 0.05. On the other hand, the 3/2/12, 6/5/12, 7/18/12, and 10/14/12 dates have daylight hours from 11 to 14 hours, so the ten hour window did not consider 30 minutes to two hours immediately before sunset and after sunrise. Figure 4.2b shows the MBE results. Again, the overall MBE is sometimes outside of the +/- 0.05 goal, but when smaller windows of the day around noon are considered, the overall MBE is always within the goal. It is interesting to note that the MBE is generally largest in magnitude at solar noon (blue), and decreases as the window is opened from 2 hours around solar noon to 5 hours around solar noon.

Figure 4.3a shows an example of a well-fit day, while Figure 4.3b shows one of the least well-fit days. Note that the selected station in Figure 4.3a for 3/2/12 may be slightly tilted to the east, exhibiting higher morning irradiance and lower afternoon irradiance. Otherwise, the peak and shape of the curve are well fit.

www.manaraa.com

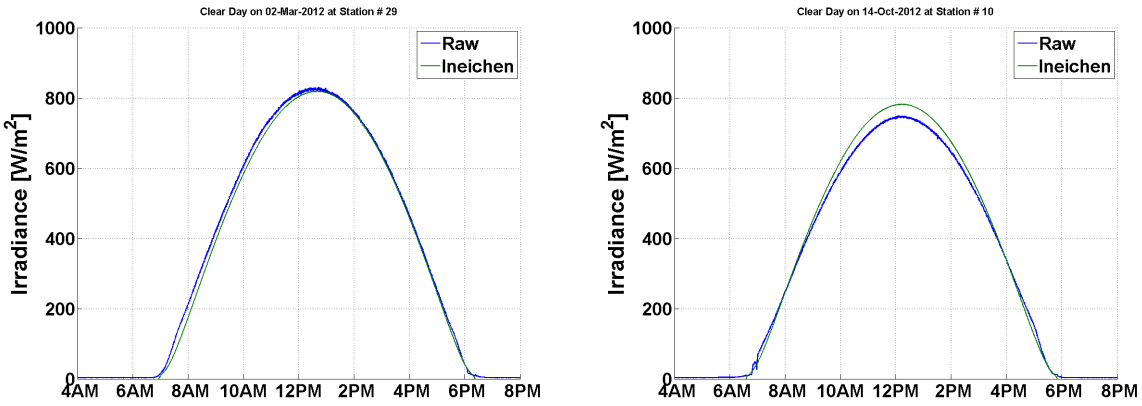

(a) 03/02/12 (b) 10/14/12

Figure 4.3: The final clear sky model generally fit the measured irradiance well, although some times of the year (i.e. March) were better fit than others (October).

Figure 4.4 shows the difference in solar noon irradiance over the 10 minute window before and after solar noon between the measured value and the clear sky model. The maximum irradiance error is just over 40 W/m^2 .

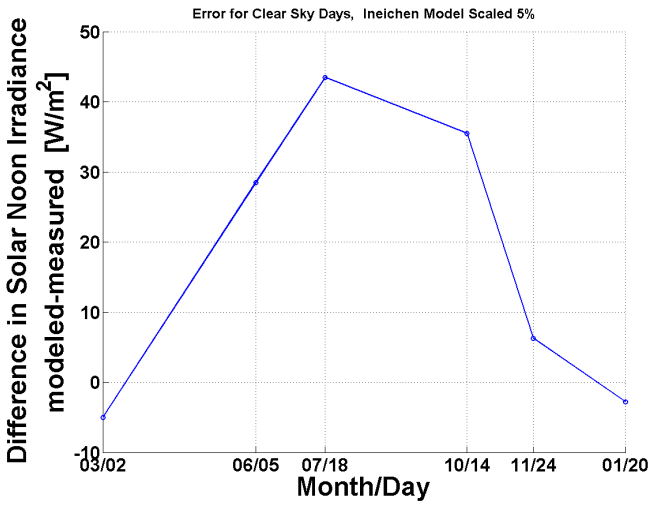

Figure 4.4: The difference between the final modeled clear sky irradiance and measured irradiance was within 45 W/m^2 at solar noon on all six of the clear days tested.

www.manaraa.com

The Ineichen clear sky model selected was calibrated to meet the specified criteria. The Ineichen model uses the standard Linke Turbidity values (from the database) and is calibrated by derating the irradiance by 5%. The result is that the model is within about 40 W/m^2 of the reference irradiance for each of the six selected clear days in the dataset and the daily average Root Mean Square Error and Mean Bias Error is always less than 0.05 when considering the 10 hour period around solar noon. Further improvements could be made to this calibration by considering a combination of TL and scaling; i.e. the TL values could be adjusted seasonally and then a scaling factor could be applied. This might further improve the model as the model's fit to measured data does appear to depend on time of year.

4.1.2 VI calculation

The Variability Index (VI) as introduced in Section 2.3.5 can be calculated at any timescale desired between time resolution of the measured data (one second in this case) up to one day. The VI chosen for use in this study is the daily VI value calculated from one-minute averages of irradiance measurements and calculated clear sky values. This timescale was chosen to reflect the variability on a relatively short one-minute timescale. Figures 4.5a and 4.5b shows the irradiance on two days with extreme irradiance values (from very low to very high in terms of one-minute VI) A VI of one indicates a clear day, while a VI of 23 indicates a highly variable day. Figures 4.6a and 4.6b show two days with medium variability. (These two days will be examined in more detail in this project because they have similar variabilities but significantly different spatial smoothing effects.)

www.manaraa.com

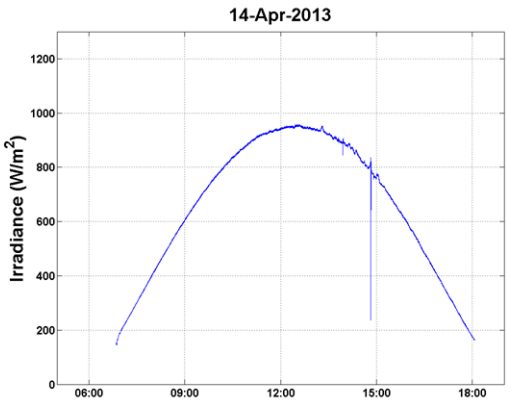

(a) April 14: VI=1

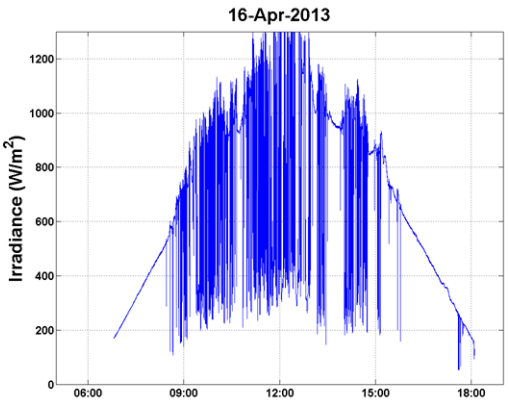

(b) April 16: VI=23

Figure 4.5: April 14 and April 16, 2013, represent two days which with variability on the extremes: April 14th has a VI of 1, April 16th has a VI of 23.

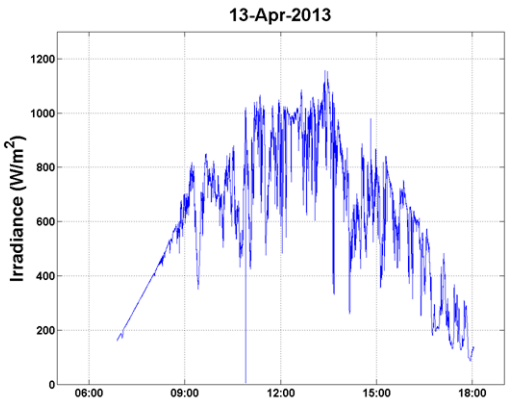

(a) April 13: VI=11

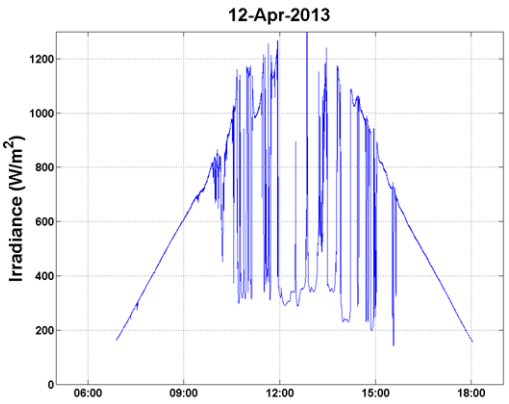

(b) April 12: VI=13

Figure 4.6: April 13 and April 12, 2013 represent two days which with medium variabilities, having a one-minute VI of 11 to 13.

4.1.3 Regulation and sub-regulation signal detection

The concepts of regulation and sub-regulation signals were discussed in Section 2.2.

While these definitions of regulation and sub-regulation are generally accepted, there

www.manaraa.com

is no industry standard way to separate regulation and sub-regulation from power signals. The algorithms used here are those implemented by Willy [12] and Flood et al., [11]. First, the changes in power output that would be handled by load-following are estimated by ten-minute block averages of the power output. Then, any changes that must be handled on the regulation timescale are estimated by subtracting the one-minute block averages from the linear trend between the ten-minute averages. Finally, any changes that must be handled on a sub-regulation timescale are estimated by subtracting the one-second data from the linear trend between the one-minute averages. This is illustrated in Figure 4.7. Using this method, the regulation timesignal has one-minute resolution and the sub-regulation timescale has one-second resolution.

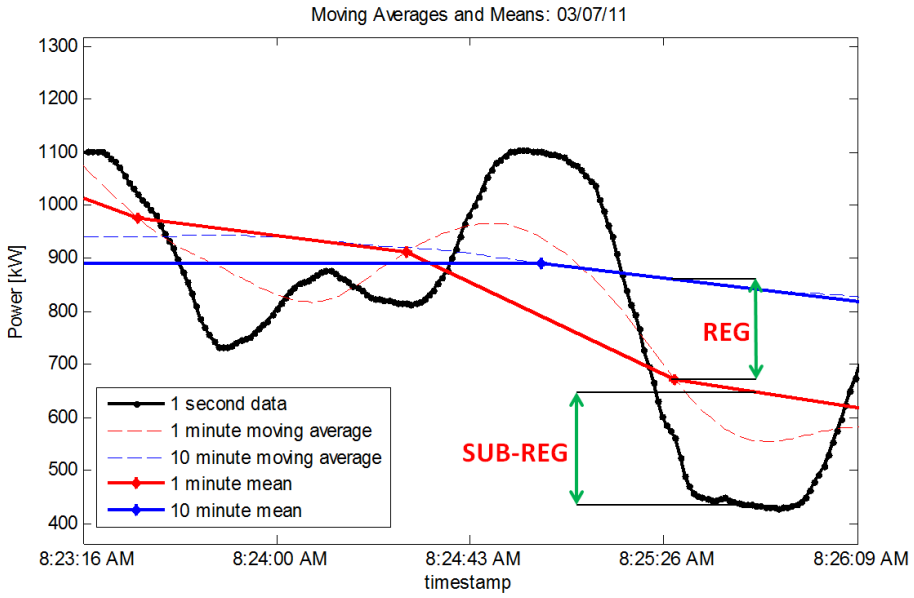

Figure 4.7: An algorithm was used to detect regulation and sub-regulation signals [12]

www.manaraa.com

4.1.4 Ramp detection

As discussed in Section 2.3.6, no single definition of irradiance (or power) ramps exists. Here the deadband algorithm is selected to detect ramps per Willy [12]. The sensitivity of the algorithm is set by choosing a deadband size, which will determine the size of the event that is considered a ramp. The selection of this algorithm and the sensitivity level chosen essentially define what will be considered a ramp in this study; anything detected by the calibrated algorithm is considered a ramp. This ramp definition is therefore affected by the subjective judgment by the user, so it is acknowledged that the ramp results provided in this work are completely dependent on the ramp definition chosen. This section serves to document the ramp definition.

The deadband ramp detection method defines a ramp to be a set of irradiance data points where a linear estimation of the irradiance between the first and last datapoint is within the deadband value of every data point between the first and last points. Figure 4.8 shows the first point "Turning point" and the last point "New turning point" of a ramp. The vertical red bars indicate the deadband above and below each point. The line connecting the first point and "New Point" does not fall within the deadband value of all of the points in between, so this line is not a ramp event and the new point will be the start of a new ramp. Therefore the deadband value (in W/m^2) sets the sensitivity of the algorithm. If the deadband value is small, the ramps will be short (several seconds long) events, while if the deadband value is large, the ramps could include longer events.

www.manaraa.com

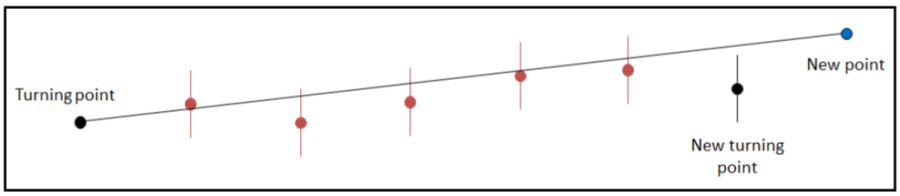

Figure 4.8: The deadband ramp detection algorithm uses a deadband around each irradiance measurement to determine when a ramp starts and ends [12]

An algorithm was implemented in MATLAB to detect the ramps. This algorithm was created by Willy and is documented in [12]. In order to select the desired sensitivity, the algorithm was run on several test days with different deadband values. Figure 4.9 shows three different deadband values tested on a variable irradiance day in June 2012. The 5 W/m^2 deadband value (top), when implemented over one week around this date, detected 22,296 ramps. The 25 W/m^2 deadband value detected 5,931 ramps, and the 100 W/m^2 value detected 1,026 ramps over one week. In order to determine which sensitivity level was desired for this work, the ramps detected were visually inspected over shorter periods of time. Figure 4.10 shows a fifteen minute period on the same day. The 25 W/m^2 deadband (middle) was preferred over the 100 W/m^2 deadband (bottom) because it follows the irradiance changes at a short timescale well where the 100 W/m^2 deadband only captures changes that are more than a few minutes long. Compared to the 5 W/m^2 deadband, the 25 W/m^2 deadband picks out the significant ups and downs on a 0-5 minute timescale without considering every new point the start of a new ramp. Other deadband values were also tested and other example days were considered. The 25 W/m^2 deadband value was chosen for irradiance ramps because it will provide ramp information on timescales of interest for this study.

www.manaraa.com

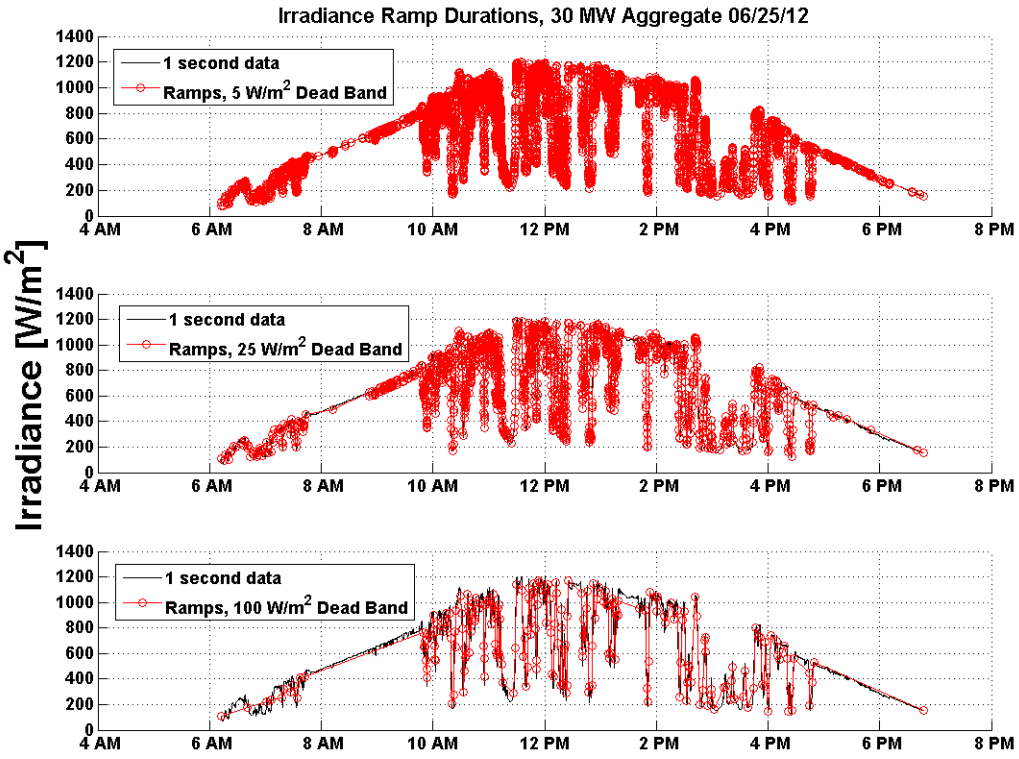

Figure 4.9: A comparison of selected deadband values for 06-25-12 shows that the 15 W/m^2 deadband was overly sensitive to changes in irradiance while the 100 /deadband 'missed' small ramps.

www.manaraa.com

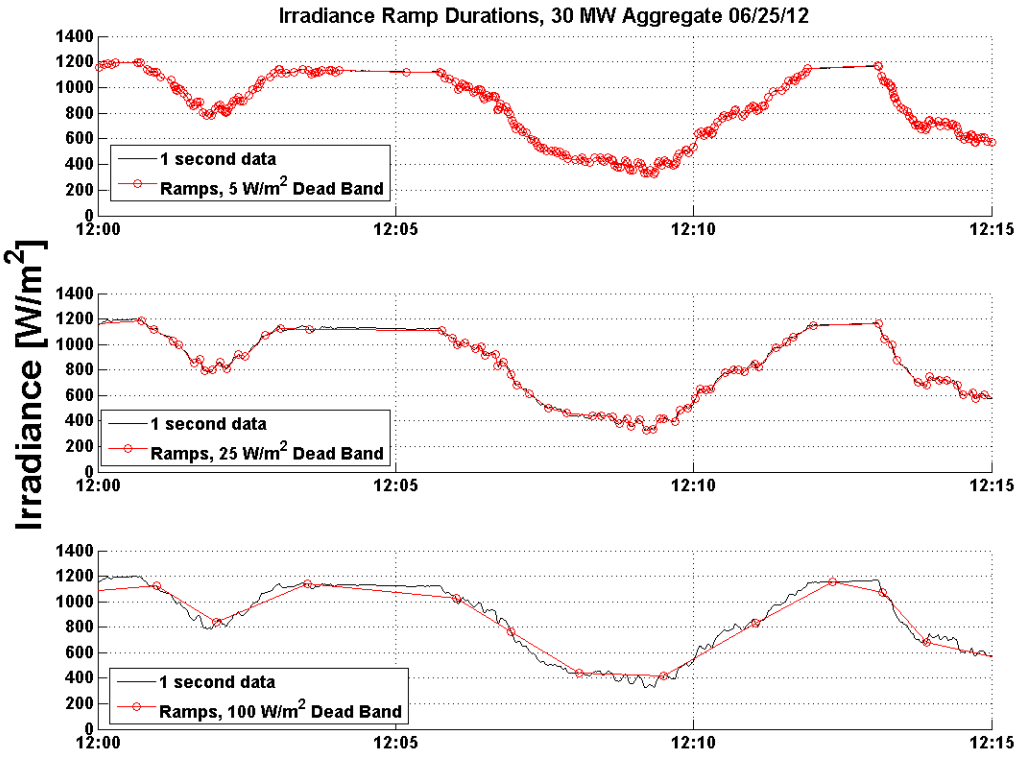

Figure 4.10: A comparison of selected deadband values over 15 minutes for 06-25-12 shows that the 25 W/m^2 deadband detected the ramps which were of interest in this study.

In addition to calibrating the irradiance ramp detection algorithm, the regulation and sub-regulation ramp detection algorithms also had to be separately calibrated. The regulation ramps were detected using a 17.5 W/m^2 deadband and the sub-regulation ramps were detected using a 2.5 W/m^2 deadband.

www.manaraa.com

4.2 Implementation of the Wavelet Variability Model

The Wavelet Variability Model was implemented using the GUI-based MATLAB program discussed in Section 2.7.3. The model's inputs are single-station solar irradiance, daily A-value, location of PV power plant, and size of PV power plant. This section summarizes the selection of four representative time periods for the analysis and describes how the A-values were calculated for the representative periods.

4.2.1 Selection of representative periods

Four periods were selected which represent the variety of variability conditions which can occur throughout the year at this location. In order to select representative periods, the daily VI was calculated over an entire year as shown in Figure 4.11. By examining the 365 day trend, rough cutoffs were selected for VI categories; the lowest daily VI values seen were between 1-2 and the highest daily VI values seen were over 15 (a few days were over 20). In between these cutoffs, variability categories were chosen to cover daily VI values of between 5 and 10, and between 10 and 15. Four one-week periods were selected that had a weekly average of VI that corresponded to these categories. Within any period there are single days that may be more or less variable than the period is on average, but the period as a whole represents real conditions would be seen in a week at this site.

www.manaraa.com

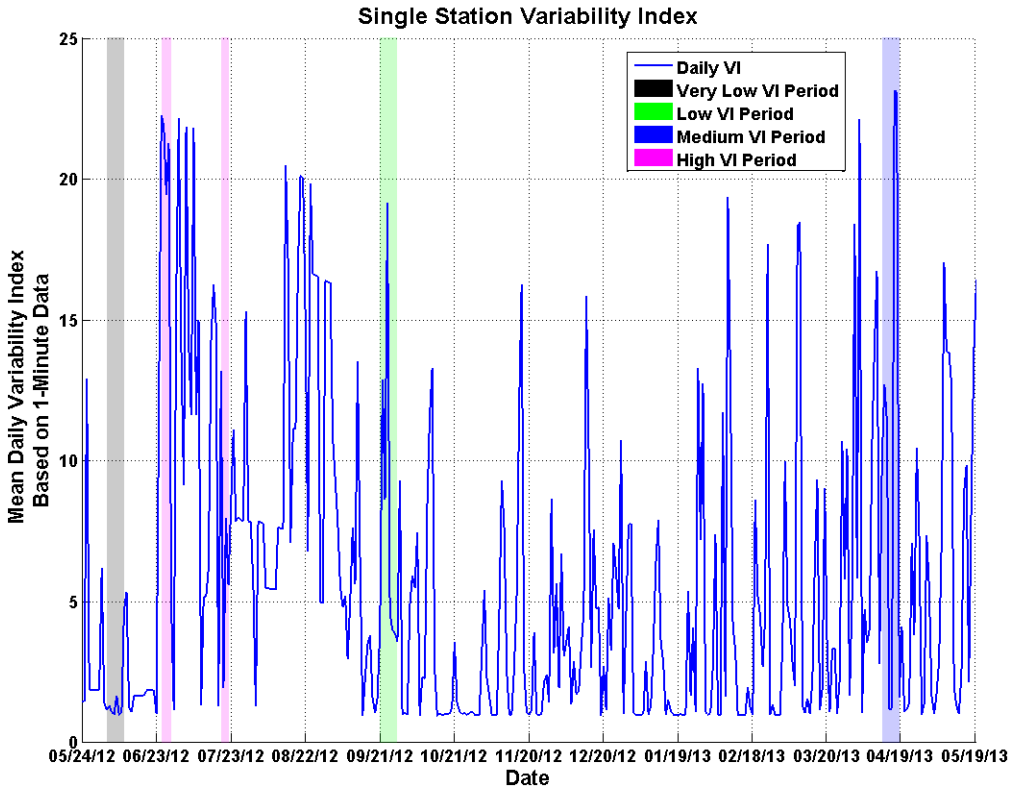

Figure 4.11: The daily VI values were examined over one year to select four representative VI categories.

The Very Low VI category (grey in Figure 4.11) was a clear period during the summer. The Low VI category (green) was a fall period with an average daily one-minute VI value over the seven days of 8.17. The Medium VI category (blue) was a spring period, and the High VI category (magenta) is a monsoon-like period. Because these highly variable monsoon periods also meant limited solar irradiance for the charging of the stations in the field, this seven-day period was composed of two separate three and four-day periods in order to choose days that had high variability and also had good data availability. Table 4.2 summarizes the VI values and dates of

www.manaraa.com

the selected periods.

Table 4.2: Four seven-day periods were chosen to represent the range of variability conditions that typically occur at the project site.

Category	Mean Daily VI (1-minute VI)	Dates
Very Low	1.19	6/3/12 - 6/9/12
Low	8.17	9/21/12-9/27/12
Medium	11.8	4/11/13-4/17/13
High	15.4	6/25/12-6/28/12 and 7/19/12-7/21/12

4.2.2 Calculation of correlation scaling coefficient

An important input to the WVM model is the correlation scaling coefficient. For every day of interest (all of the dates in the four selected VI categories), the available data was used to determine an A value for each date. As discussed in Section 2.7, A is a scaling coefficient in the relationship between the correlation of clear sky index changes at two sites, distance between the sites, and timescale. The relationship is:

$$\rho = \left(exp^{\left(\frac{-d_{m,n}}{t}\right)} \right)^{\left(\frac{1}{A}\right)} \tag{4.3}$$

Figure 4.12 shows an example of how the correlation scaling coefficient is determined. For all of the available irradiance sensors on this date, the clear sky index change time series for multiple time scales were first calculated. Next, the correlations between station pairs for every timescale was determined. Finally, an A-value is determined which gives the best fit to the relationship in Equation 4.3. For the example in Figure 4.12 the A-value was determined to be 7.1. Lines for A=20 (a more highly correlated day) and A=4 (a less correlated day) are also shown.

www.manaraa.com

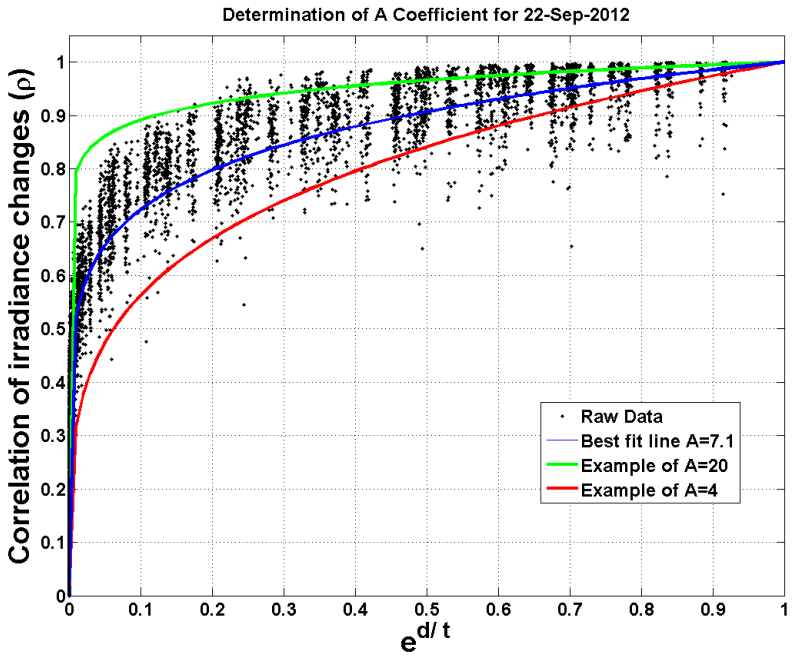

Figure 4.12: The A Value was determined by fitting a line to data from the 45 sensor network.

The correlation scaling coefficients for each date are provided in Table 4.3 along with the associated VI values. It is important to differentiate between the meaning of VI and A. The VI value indicates the variability of the irradiance and the A value indicates the strength of correlation of irradiance changes as a function of distance and time. Therefore, there is no direct relationship between A values and VI values. The only significant trend is that days with low VI (clear days) tend to have low A values. Days with medium to high VI could have very low A value (uncorrelated sites), or a very high A value (correlated sites). It is not at first obvious that clear days have low A values. Intuitively, clear days would mean that stations would all be well correlated; all seeing the same smooth irradiance profile over the day. However, the low A value is calculated because when there are essentially no changes in short term

www.manaraa.com

irradiance, any small changes which come about due to measurement resolution are 'seen' as significant changes and show that the stations are not correlated. However, it is of no importance in application because when an A value of any magnitude, low or high, is applied to a clear day's irradiance, any 'smoothing' of the irradiance only makes a clear day's irradiance even more clear or smooth. Essentially there is no change that is of interest in studying solar PV power when running a clear day's irradiance through the Wavelet Variability Model.

www.manaraa.com

Table 4.3: Correlation scaling coefficient and daily VI for selected dates

Date	A value	VI Category	Average of 1-Minute Variability Index (VI)
3-Jun-12	0.3	Very Low	1.2
4-Jun-12	2.1	Very Low	1.3
5-Jun-12	5.3	Very Low	1.1
6-Jun-12	0.9	Very Low	1.0
7-Jun-12	1.4	Very Low	1.7
8-Jun-12	0.8	Very Low	1.0
9-Jun-12	4.6	Very Low	1.1
21-Sep-12	0.9	Low	4.1
22-Sep-12	7.1	Low	12.9
23-Sep-12	11.5	Low	8.6
24-Sep-12	9.6	Low	19.1
25-Sep-12	7.0	Low	4.6
26-Sep-12	1.2	Low	4.0
27-Sep-12	1.8	Low	3.9
11-Apr-13	10.9	Medium	10.0
12-Apr-13	3.3	Medium	12.7
13-Apr-13	20.0	Medium	11.4
14-Apr-13	0.3	Medium	1.2
15-Apr-13	1.7	Medium	1.2
16-Apr-13	4.4	Medium	23.1
17-Apr-13	7.0	Medium	23.1
25-Jun-12	4.7	High	22.2
26-Jun-12	5.0	High	21.9
27-Jun-12	8.9	High	19.4
28-Jun-12	3.8	High	21.2
19-Jul-12	5.4	High	13.2
20-Jul-12	5.4	High	1.9
21-Jul-12	9.2	High	8.0

Figure 4.13 and Figure 4.14 illustrate the difference between highly variable, uncorrelated days, and highly variable, correlated days. In this example, both dates appear to have similar variability, and both have similar 1-minute VI values. However, the A-value on November 1st is low, while the A-value on April 10th is high. In Figure 4.14, when a closer view of the irradiance from 1PM to 2PM is taken, it is

www.manaraa.com

clear that the irradiance changes on April 10th occur at about the same time over all of the sensors in the field. However, on November 16th, the irradiance changes are more random; one station does not necessarily see the same change as another. This means that although these dates have relatively similar point irradiance variability, the power output over the PV plant on November 16th would have a much smoother profile, because the irradiance changes are seen at different times by different sensors, resulting in an overall more smooth average irradiance profile. Both conditions do occur and the WVM is especially adept at representing them both through the A-value.

www.manaraa.com

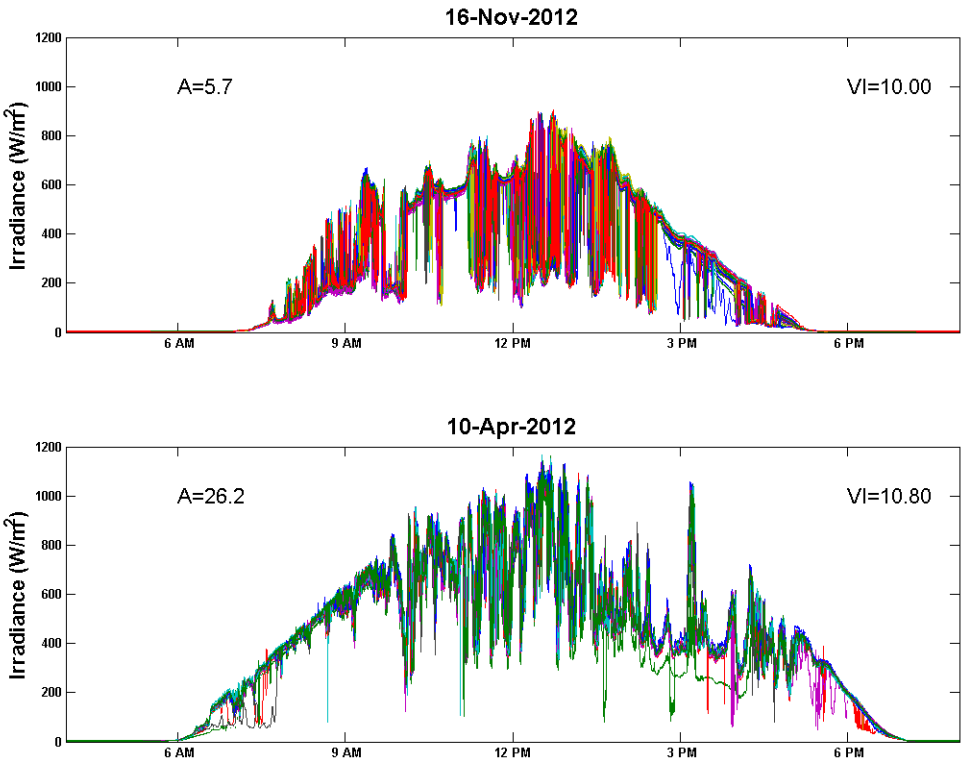

Figure 4.13: Two days with similar variability (VI approximately 10) can have different A values.

www.manaraa.com

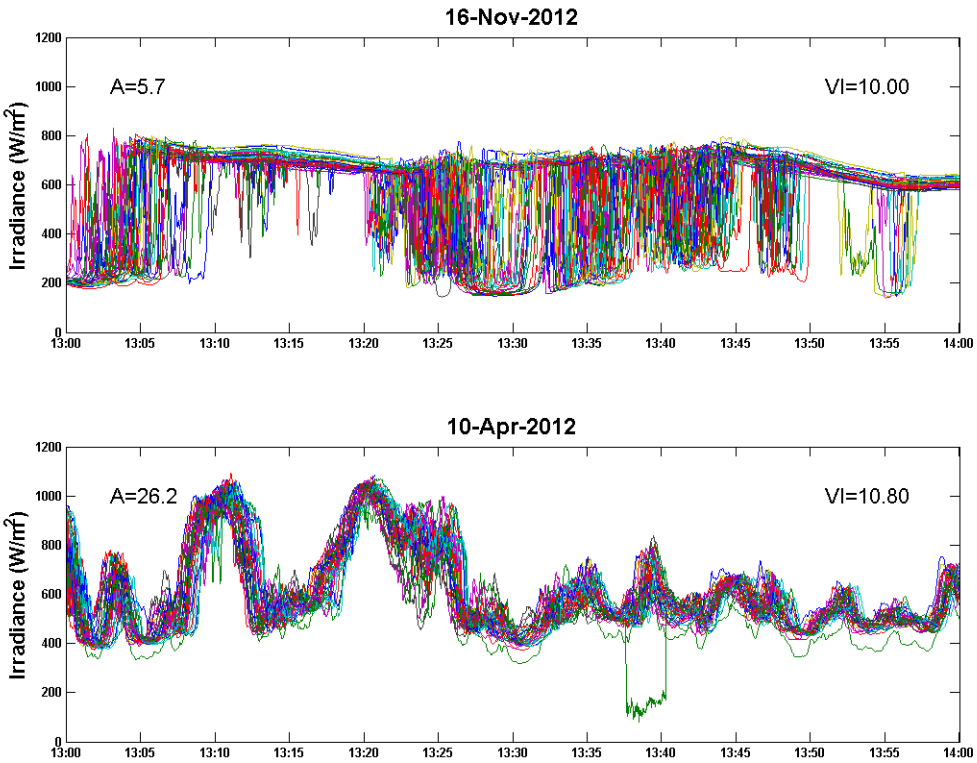

Figure 4.14: The irradiance over one hour on two days with similar variabilities shows that a day with a high A value (bottom) has stations that are well-correlated, while a day with a low A value (top) has stations which are not well correlated.

4.3 Results

This section summarizes the results of the analysis which are used to answer the three primary research questions for this thesis.

www.manaraa.com

4.3.1 Spatial smoothing: Modeling smoothed irradiance for representative periods

The first research question of interest in this work was: What is the spatial smoothing of irradiance that occurs over a distribution scale PV power plant and a transmission scale power plant? This section provides the variability analysis to answer this question. The variabilities of irradiance determined from a single point sensor, the WVM, and an aggregate irradiance from the network of sensors are compared for both a distribution scale and transmission scale power plant.

The WVM was applied for the four week-long periods selected representing the four different VI categories. For each of these periods the WVM was applied twice; once to model the smoothing over a 10 MW plant, and once to model the smoothing over a 30 MW plant. Similarly, the averaged "aggregate" irradiance is applied for each of the four weeks, once for the 10 MW plant and once for the 30 MW plant. The aggregated irradiance was determined from a simple average of the sensor irradiance. For a 10 MW plant, this was a simple average of the 1-second data from the nine inner stations. For the 30 MW plant, this was a simple average from the 25 inner stations. These sensor layouts are shown in Figure 3.1. Note that although there were times when not every station was available, the days selected for this analysis were chosen to maximize uptime so that a majority of the stations were available for the analysis. The single station (unsmoothed) irradiance was also considered for each time period. There are a total of 20 different week-long irradiance datasets.

Then, to analyze the variabilities for all 20 of the different datasets, the raw irradiance, the irradiance ramps, regulation time series, sub-regulation time series, regulation ramps, and sub-regulation ramps were compared. Table 4.4 summarizes

www.manaraa.com

all of the different analysis that were completed.

Table 4.4: 20 irradiance results were anlyzed for each of the four VI periods and 5 smoothing methods.

Single station irradiance	Very Low VI	Low VI	Medium VI	High VI
10 MW Aggregate				
10 MW WVM				
30 MW Aggregate				
30 MW WVM				

Irradiance results

The irradiance results are provided here for two example days in the Medium VI period during April 2013. April 12th has a VI of 12.7, and an A-value of 3.3. The raw irradiance is compared to smoothed irradiance modeled by the aggregate in Figure 4.15a. Figure 4.16a shows one hour of this day in more detail. The raw irradiance is compared to WVM smoothed irradiance in Figures 4.15b and 4.16b. Whether using the aggregate model or WVM model, the 30 MW power plant appears more smooth than the 10 MW plant due to plant size. Using the WVM model, however, appears to provide more smoothing than the aggregate model because the WVM irradiance signal does not exhibit the rapid fluctuations in irradiance that the aggregate irradiance signal does. This 'appearance' of smoother irradiance will be confirmed by using the VI and ramp analysis to quantify variability in the next sections.

Another example day is considered on April 13, which has similar variability to April 12 (VI=11.4 for the 13th). This day has much less smoothing based on the A value (A=20 compared to 3.3 for April 12). Figures 4.17a through 4.18b can be compared directly to Figures 4.15a through 4.16b to see that the smoothing is much

www.manaraa.com

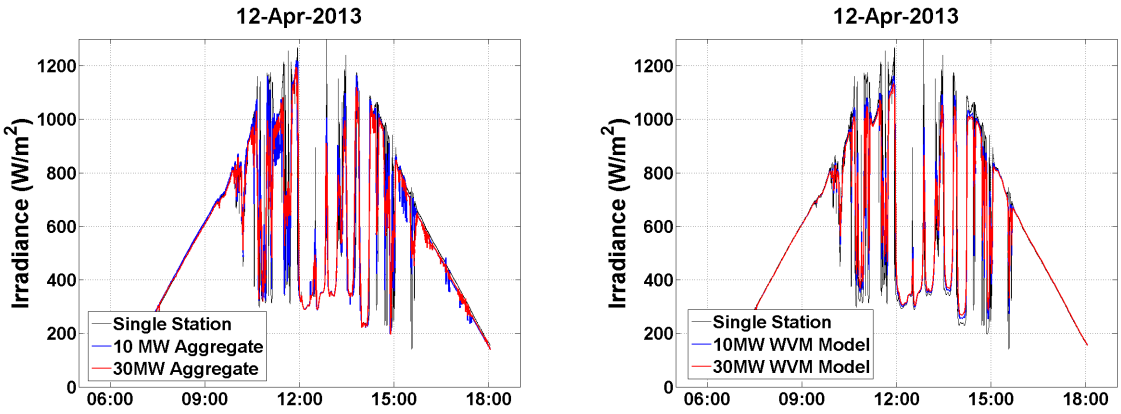

(a) Aggregate model (b) WVM

Figure 4.15: Smoothed irradiance using WVM and aggregate model for April 12, 2013 (VI=12.7, A=3.3) appears similar over the course of a day.

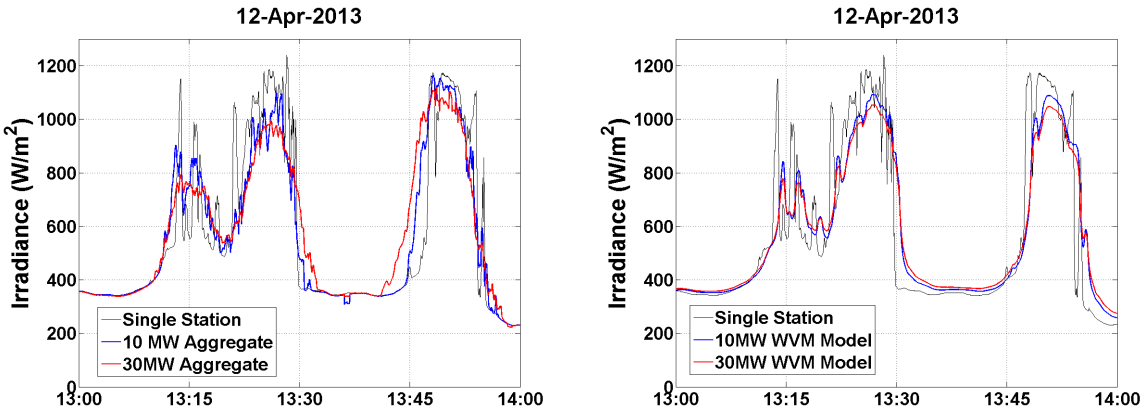

(a) Aggregate model (b) WVM

Figure 4.16: Smoothed irradiance over one hour using WVM and aggregate model for April 12, 2013, is very different on a sub-hour timescale between the aggregate model and WVM.

less significant on April 13th than on April 12th. The smoothed irradiance from the aggregate model and WVM model appear similar, and both are similar to the single station irradiance, at least when considering the irradiance over a one hour period.

www.manaraa.com

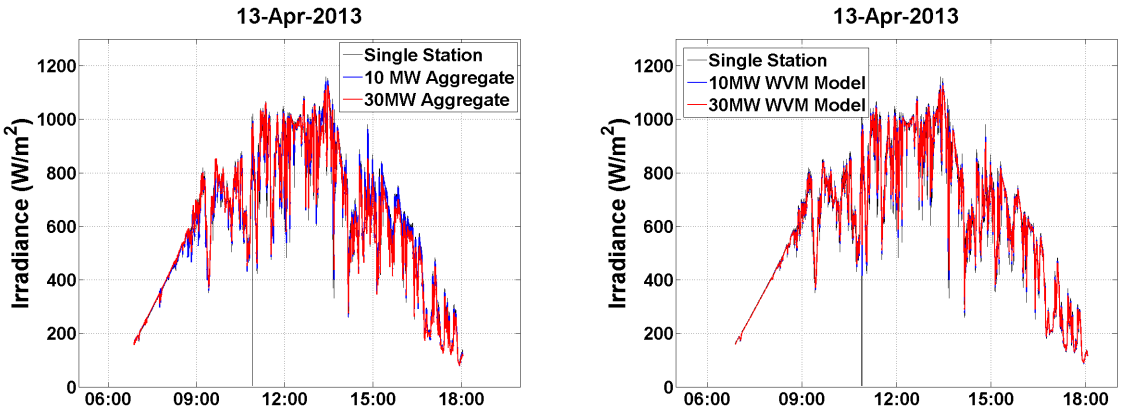

(a) Aggregate model (b) WVM

Figure 4.17: Smoothed irradiance using WVM and aggregate model for April 13, 2013 (VI=11.4, A=20.0) appears the similar regardless of the model used or the size of the power plant.

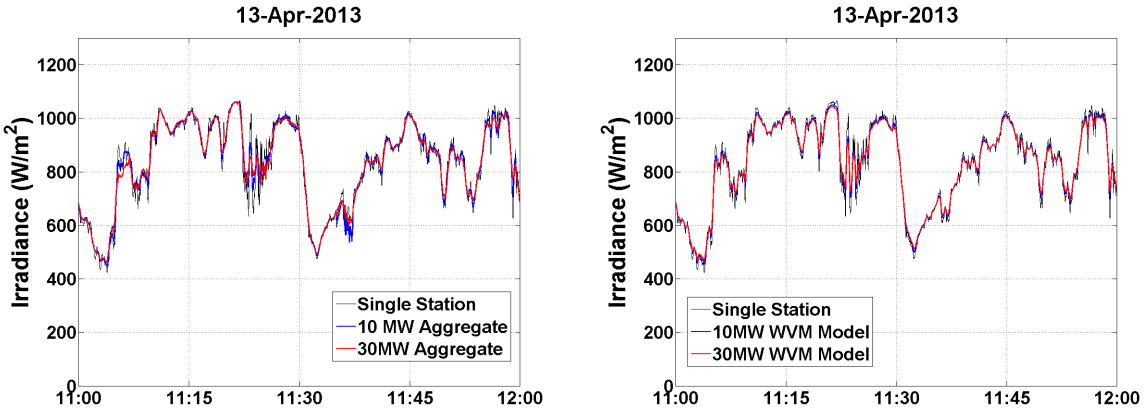

(a) Aggregate model (b) WVM

Figure 4.18: Smoothed irradiance over one hour using WVM and aggregate model for April 13, 2013 appears to be the same regardless of the model used or the size of the power plant on a sub-hourly timescale because the day has a high A value (20.0).

Variability Index results

The VI results are examined for the four periods for the two irradiance smoothing models and compared to the single station irradiance VI. Figure 4.5 shows how the

www.manaraa.com

average of the seven day's daily one minute VI changed for each smoothing method. The period averaged VI is smoothed more (has lower VI) for the 30 MW plant size than for the 10 MW plant size, and the WVM predicts lower VI than the aggregate model. Figure 4.6 shows the VI results for each of the 28 days listed in this case in order of daily single station VI instead of VI category. This figure shows how smoothing changes the VI value. For days with very low VI (about 1), the smoothing that occurs is not important because the smoothed VI values are still approximately 1. However, for days with higher VI values, the smoothed VIs are always decreased by some amount compared to the single station VI value. One notable exception in both figures is that for very low periods, the aggregate model sometimes predicts more variability than the single point sensor (anti-smoothing). This is examined and explained in Section 4.3.1.

Table 4.5: A comparison of the average of daily VI values by variability period and smoothing method shows that the two models give similar smoothed VI results over the course of a week.

VI Period	Single Station	10MW Agg	30MW Agg	10 WVM	30 WVM
Very Low	1.1	1.1	1.2	1.0	1.0
Low	11.9	10.3	9.0	9.1	8.1
Medium	16.8	15.2	13.0	12.7	11.2
High	25.2	21.2	17.6	20.2	17.8

VI Color Key	Very Low	Low	Medium	High

The amount of smoothing which occurs depends on the size of the plant and the daily weather conditions as represented by the A-value. Figure 4.19 shows the percent decrease in VI from a single sensor irradiance to smoothed irradiance vs the A-value.

www.manaraa.com

Table 4.6: A comparison of the daily VI values, ordered by variability, show that the aggregate model and WVM have slightly different smoothed VI results.

Date	A-value	Single Station VI	10MW Aggregate VI	30 MW Aggregate VI	10 MW WVM VI	30 MW WVM VI
28-Jun-12	3.8	41.3	36.4	28.5	38.2	34.4
27-Jun-12	8.9	37.8	37.2	32.2	35.2	31.8
16-Apr-13	4.4	36.1	33.6	29.0	22.8	18.3
25-Jun-12	4.7	34.5	25.4	21.2	21.7	18.4
17-Apr-13	7	32.2	28.0	23.1	26.1	23.4
26-Jun-12	5	29.8	24.3	19.9	22.0	19.0
24-Sep-12	9.6	27.8	26.1	23.6	23.2	21.0
22-Sep-12	7.1	19.2	16.0	13.4	15.8	14.3
19-Jul-12	5.4	17.7	13.7	11.2	12.7	11.0
12-Apr-13	3.3	16.3	12.3	9.6	11.6	10.0
13-Apr-13	20	15.6	14.9	13.9	13.7	13.0
11-Apr-13	10.9	14.8	14.1	12.2	12.8	11.9
21-Jul-12	9.2	12.4	9.1	8.3	9.3	7.8
23-Sep-12	11.5	10.5	9.6	8.8	9.4	8.8
26-Sep-12	1.2	8.1	6.9	5.4	4.0	3.2
21-Sep-12	0.9	6.0	3.6	3.3	3.0	2.4
27-Sep-12	1.8	5.8	4.6	3.6	3.5	2.9
25-Sep-12	7	5.7	5.3	4.7	4.7	4.3
20-Jul-12	5.4	2.9	2.6	2.3	2.5	2.3
15-Apr-13	1.7	1.6	1.7	1.7	1.2	1.1
3-Jun-12	0.3	1.2	1.3	1.3	1.0	1.0
14-Apr-13	0.3	1.2	1.5	1.6	1.0	1.0
7-Jun-12	1.4	1.1	1.2	1.3	1.0	1.0
4-Jun-12	2.1	1.1	1.0	1.2	1.0	1.0
5-Jun-12	5.3	1.1	1.0	1.1	1.0	1.0
9-Jun-12	4.6	1.0	1.1	1.1	1.0	1.0
6-Jun-12	0.9	1.0	1.1	1.1	0.9	0.9
8-Jun-12	0.8	1.0	1.1	1.2	0.9	0.9

VI Color Key	Very Low	Low	Medium	High

This figure does not include days with very low VI (about 1) since the smoothing that occurs on those days is not significant. As expected, with increasing A-values, the smoothing that occurs is decreased. Also, the smoothing that occurs is more for a 30 MW plant than for a 10 MW plant.

Note, the VI values shown in this section are higher than the daily VI values used for classification of the days because, for consistency across models, this analysis considers only the specific daylight hours that the WVM model uses. The WVM

www.manaraa.com

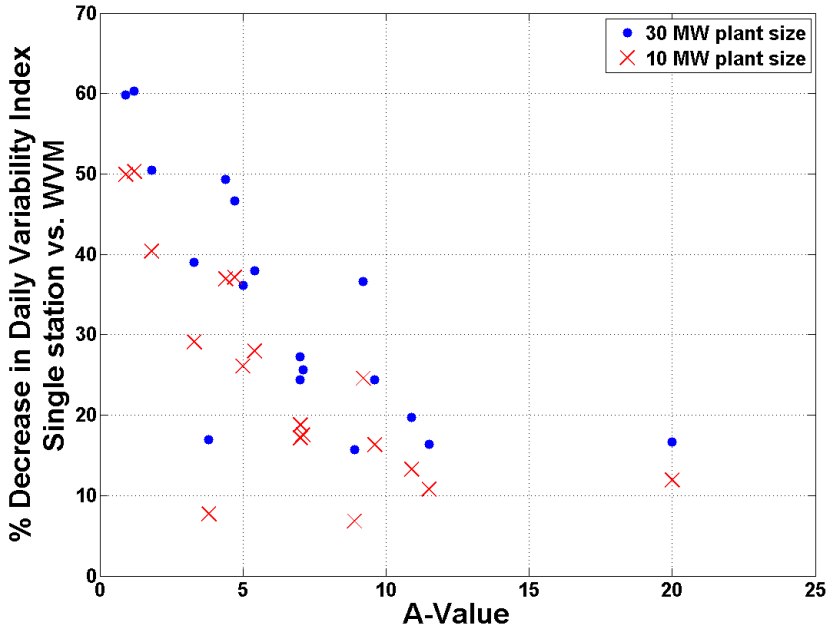

Figure 4.19: The decrease in VI between single sensor irradiance and WVM smoothed irradiance is up to 60% for days with low A values, but only about 10 to 20 % for days with high A values.

model omits less than an hour before sunset and after sunrise.

Irradiance ramp results

The irradiance ramps detected with the deadband algorithm are analyzed by looking at the ramp distribution in terms of magnitude and duration. In this section, heat maps (see Figure 4.20) are used to show what the distribution of ramps is in magnitude and duration over one week periods. In addition to this distribution of ramps, it is interesting to note the total number of ramps detected. The number of ramps detected in any irradiance time series is indicated on the heatmaps by 'N'. Finally, the extreme values of the ramps are of interest and are also examined in this section by considering

www.manaraa.com

97.5/2.5th percentiles of ramp magnitudes by ramp duration bins, corresponding the ramp magnitudes that fall within two standard deviations of the mean for normally distributed ramp durations.

The distribution of irradiance ramps detected varied significantly from single station irradiance to aggregated irradiance to WVM smoothed irradiance. Figure 4.20 shows the irradiance ramps detected during the High VI and the Medium VI periods using a single station, the aggregate model and the WVM. The aggregate models show that, as expected, the distribution of irradiance ramps changes, having fewer, short (less than five second) ramps in the case where the irradiance is smoothed using a 10 MW aggregate or 30 MW aggregate model. In addition the number of ramps (N) detected during the seven day period decreases. Figure 4.20 shows a different distribution of ramps when the irradiance is instead smoothed using the WVM. The irradiance ramps less than five seconds in duration are not only fewer, they are essentially eliminated. The number of ramps detected is significantly fewer (3,037 for WVM 30 MW model versus 5,931 for 30MW aggregate model). The ramp distribution predicted by the WVM are 'spread out' such that ramps are no longer concentrated as they are in aggregate model, but are spread over a larger range of ramp magnitudes.

www.manaraa.com

المنارة للاستشارات

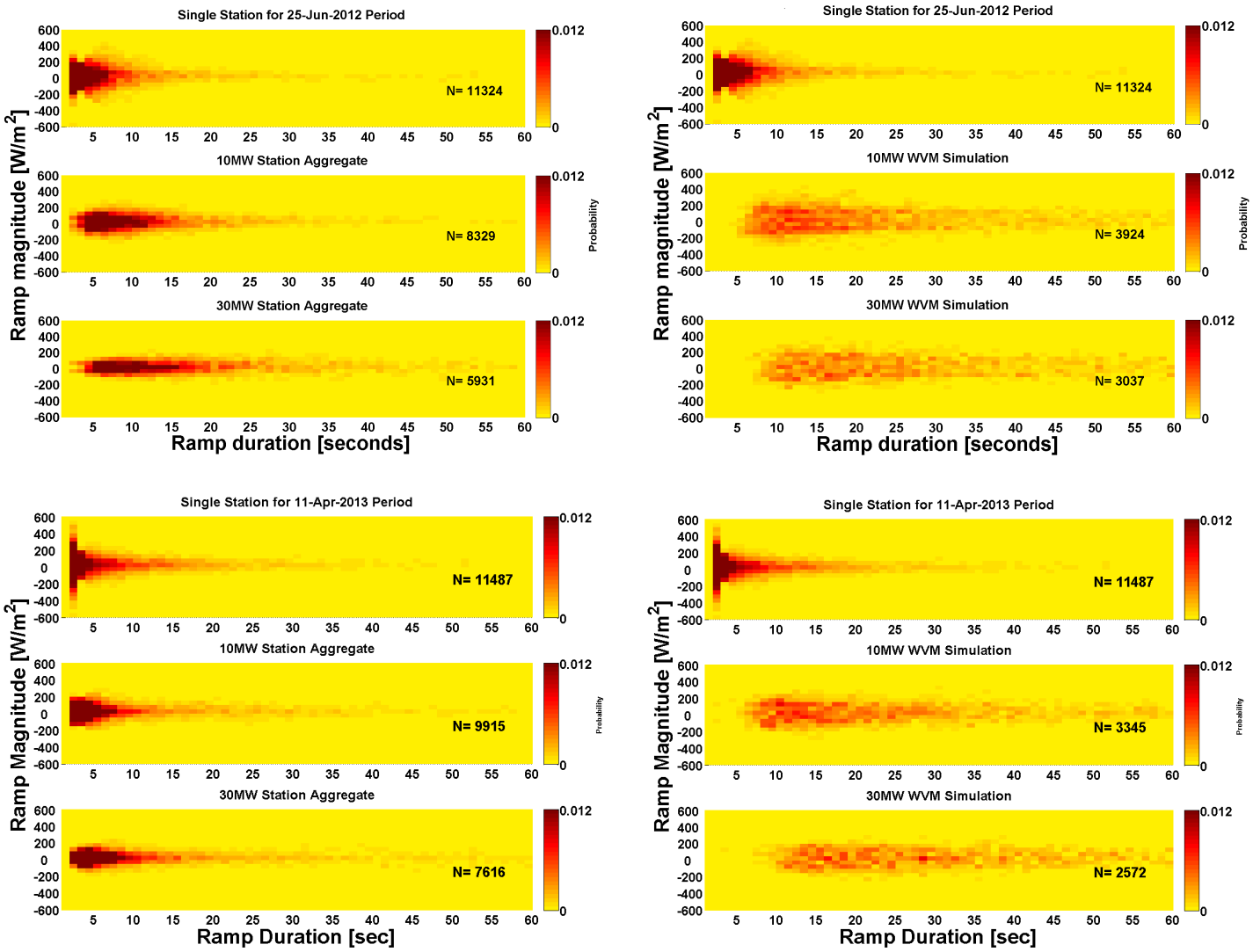

Figure 4.20: Irradiance ramp distributions for the High VI and Medium VI periods both show that the WVM results in fewer, longer duration ramps than the aggregate model.

www.manaraa.com

المنارة للاستشارات

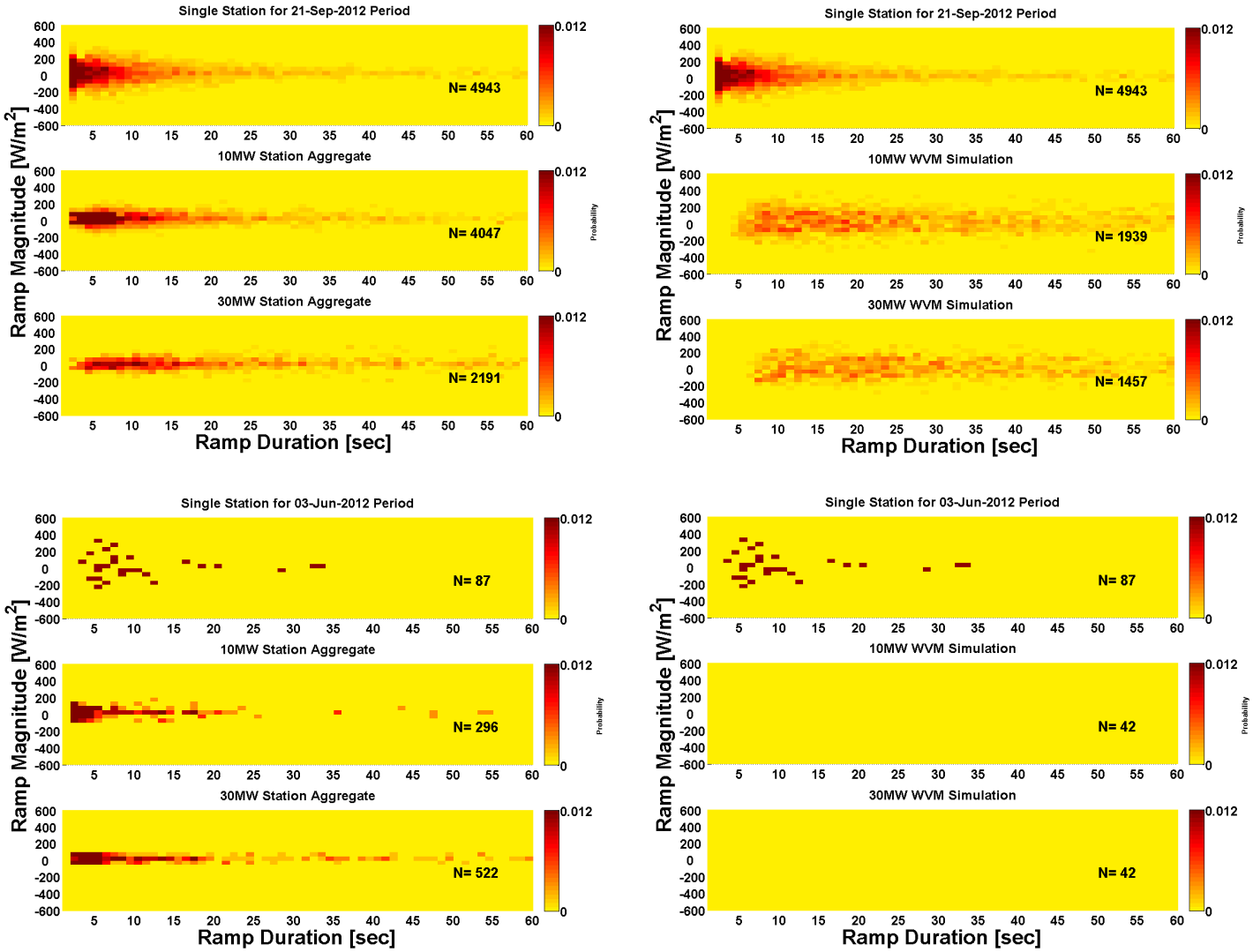

Figure 4.21: Irradiance ramp distributions for the Low VI period are similar the High and Medium VI periods, but the Very Low VI period's distributions show that the aggregate model has an 'anti-smoothing' effect.

www.manaraa.com

Figure 4.21 shows the ramp distributions for the low VI period and very low period. The Low VI period exhibits the same trends as the medium and high VI periods. However the ramp distributions for the very low VI period provide different results. The aggregation smoothing curiously shows more ramps for the 10 MW power plant and 30 MW power plant than for the single station. This was examined in more detail and it was found that the additional ramps are due to single stations seeing a short drop in irradiance during a clear period. These effects are seen more often when more than one station is used. The WVM model only uses one station as a direct irradiance input, so the effects are not seen in the model. Although it is possible that a single station could see a drop in irradiance due to a very small cloud which is only measured at one station, some examination of the data showed that it was often due to intermittent data logger operation. Figure 4.22 shows what this intermittent datalogger operation looks like. The bottom plot in the figure shows that the aggregated irradiance shows very small ramps due to this effect. Although these ramps are not consequential because their magnitude is small and they are infrequent, it is important to understand why they appear in the aggregate model. This is contrasted with the effects of actual cloud movement on a clear day, shown in Figure 4.23. In this case a cloud clearly passes over the sensors. However the number ramps detected are actually reduced due to smoothing, not increased as was seen in the heat maps of ramp distributions for the very low period. The increase in ramps in the aggregated models over the single point sensor model is a case for the WVM model because the WVM model is not subject to these singularities.

www.manaraa.com

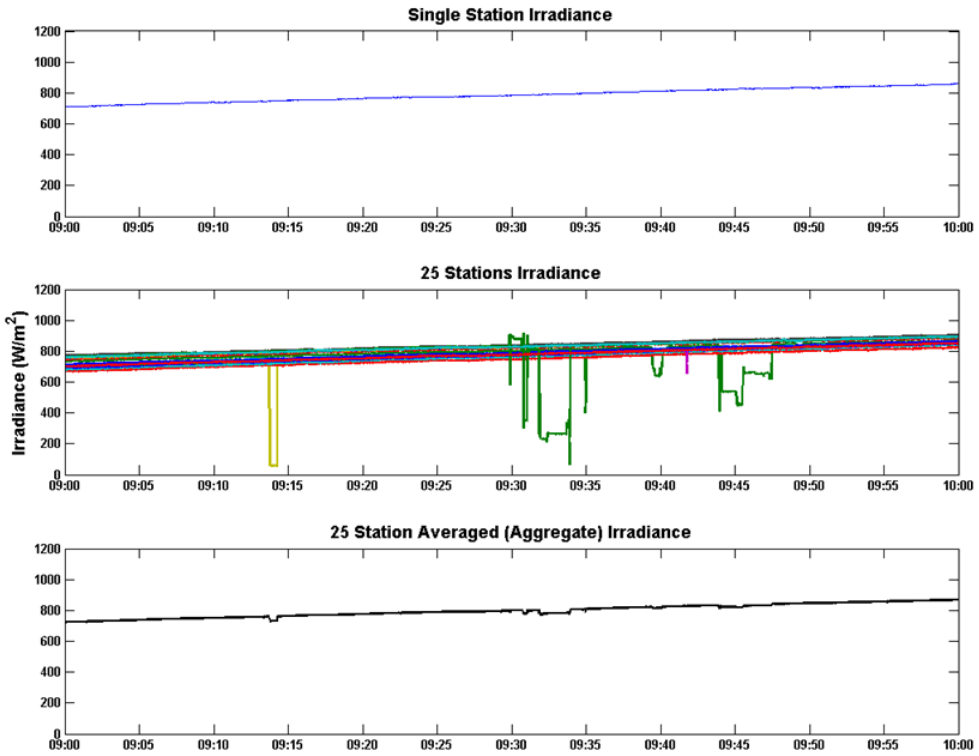

Figure 4.22: Intermittent data logger operation can cause an 'anti-smoothing' effect in the aggregate model. During a period with clear skies, intermittent datalogger operation at just one sensor (middle plot) can result in small ramps in the aggregate irradiance (bottom) which did not appear in the single sensor irradiance.

www.manaraa.com

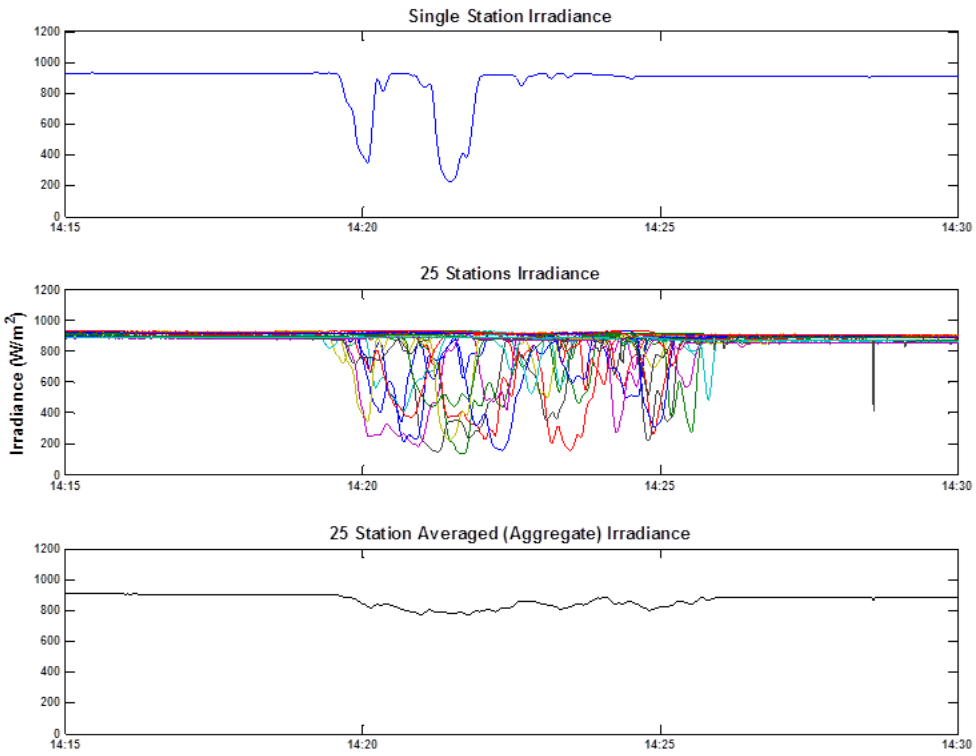

Figure 4.23: A ramp in irradiance due to true cloud motion is observed as a small cloud passes over the sensor network during a relatively clear period. The large drops in irradiance observed at one sensor (top plot) are smoothed out over 25 sensors (middle plot) and the aggregate model provides single smoothed irradiance measurement (bottom).

The WVM's predication of a 'spread out' distribution which includes some larger magnitude ramps is also evident when considering the most extreme ramp events. Figure 4.24a shows the extreme (97.5th/2.5th percentile) ramps for the single station and the aggregate models. These aggregate models predict extreme ramps for ramp durations of up to ten seconds of about 50 W/m^2 for the 30 MW aggregated model. Figure 4.24b shows that the WVM, in contrast, predicts no ramps ramps at all below

www.manaraa.com

four seconds, but predicts extreme ramp values of up to 200 W/m^2 for the 30 MW models. In summary, the WVM eliminates ramps of under a few seconds and predicts fewer, but larger ramps of longer durations. Notably the duration transition from no ramps at all to higher ramps is about five seconds in this case, but will be a higher or lower duration depending on the size of the power plant as well as the correlation scaling coefficient A.

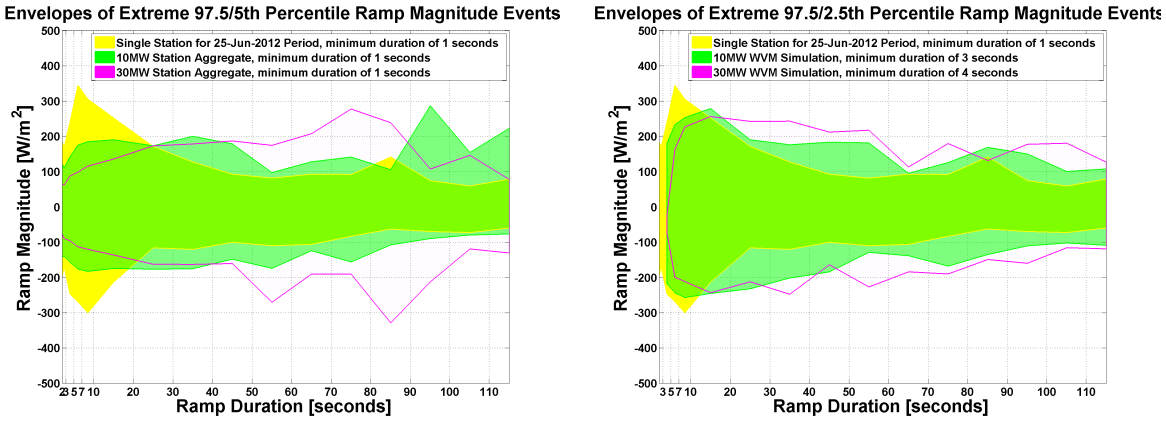

(a) Aggregate (b) WVM

Figure 4.24: A comparison of 97.5/2.5th percentile extreme ramp magnitudes by duration between the aggregate model and WVM shows that the extreme ramp magnitudes of the WVM can be larger than those predicted by the aggregate model at some durations. However, the WVM eliminates ramps of under about four seconds during this High VI period.

Complete ramp distribution statistics are provided in the Appendix for all of these periods and smoothing models.

Regulation and sub-regulation ramp results

The ramp detection algorithm, calibrated separately for the irradiance, regulation, and sub-regulation time series, is implemented on the regulation and sub-regulation

www.manaraa.com

time series. First, examination of the smoothing effects in the ramps in the regulation timescale are considered. Figures 4.25 shows that the number of regulation ramps detected and their distribution in duration and magnitude are quite similar regardless of the plant size or smoothing method. This indicates that for plants of the sizes considered here, and using the deadband ramp algorithm with a deadband of 17.5 W/m^2, most of the smoothing takes place at time scales of less than one minute. However when comparing the ramp distributions in the sub-regulation signals also shown in Figure 4.25, the results follow the pattern detected in the irradiance ramp distributions: the WVM tends to reduce (although here, as opposed to in the irradiance time series, not eliminate) the short duration ramps, and shows fewer, but larger magnitude ramps of the longer durations.

www.manaraa.com

المنارة للاستشارات

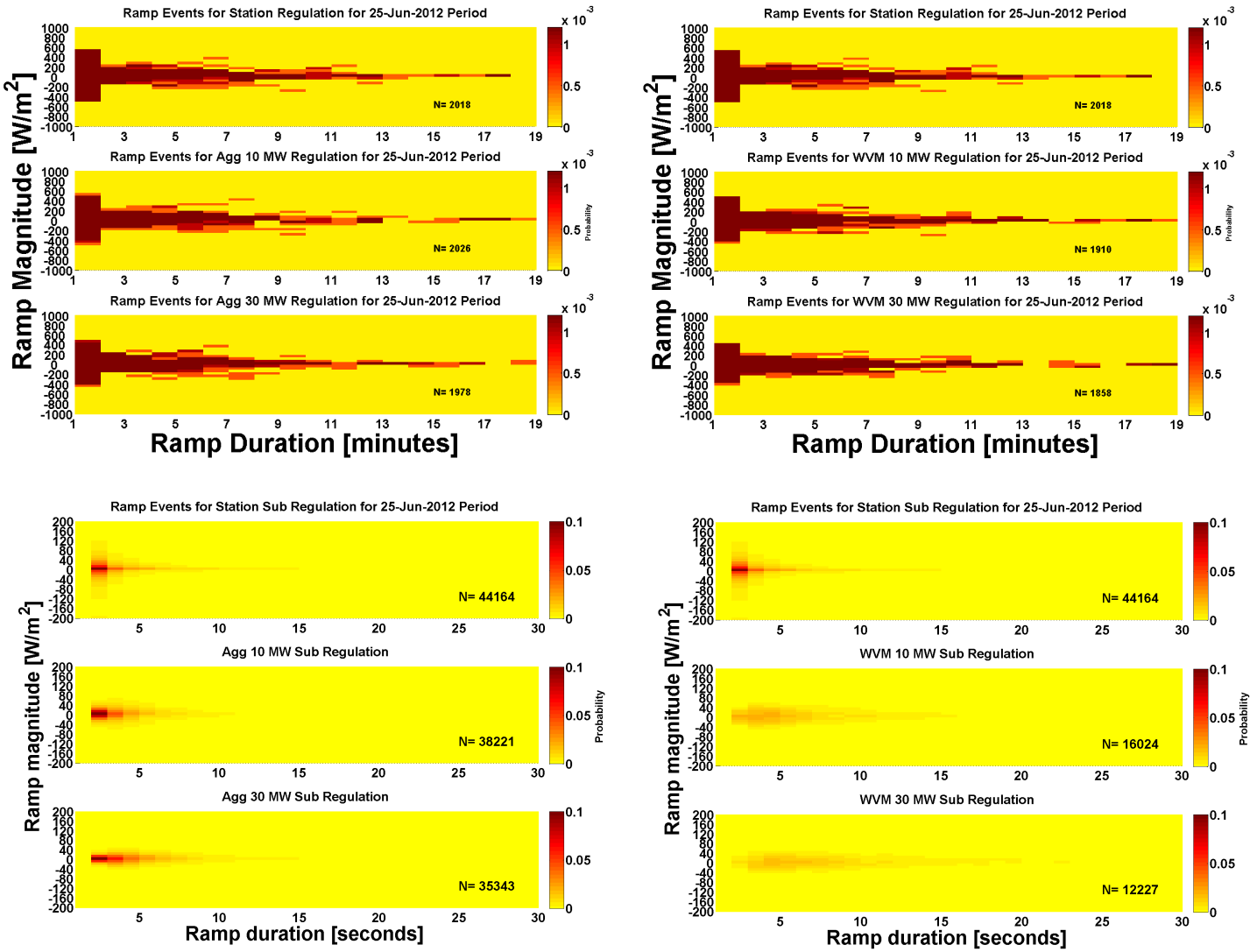

Figure 4.25: The regulation ramp distributions are similar using the WVM or aggregate model, while on the sub-regulation timescale, the WVM smoothing results in fewer, longer ramps.

www.manaraa.com

Figures 4.26a and 4.26b show the extreme (97.5/2.5th percentile) magnitudes of the sub-regulation ramps by ramp duration. As with the extreme irradiance ramps, this shows that the WVM smoothed irradiance has extreme ramps which are larger in magnitude. It is important to note, again, that the number of ramps overall is less, so although the extreme percentile magnitudes are larger with the WVM, there are fewer ramps.

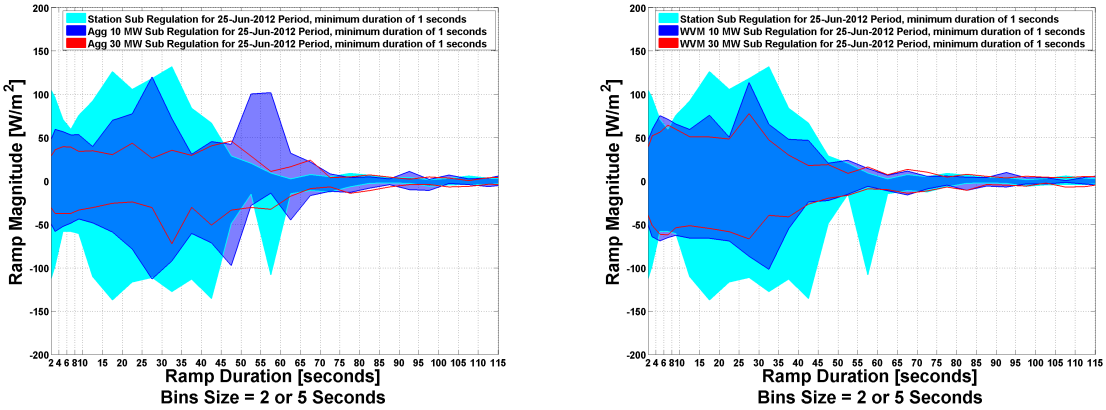

(a) Aggregate model (b) WVM

Figure 4.26: Comparison of 97.5/2.5th percentile extreme sub-regulation ramp magnitudes between the aggregate and WVM show similar trends to that of the irradiance ramps during this High VI period.

4.3.2 Spatial Sampling: Effect of number and orientation of sensors

The second question of interest in this study was: What is the best spatial sampling method to adequately represent the variability of a PV power plant?

The number of sensors and their locations needed depends on the method which is used for spatial smoothing. The key to the representation of variability in the WVM is

www.manaraa.com

the correlation scaling coefficient (A-value). In order to determine how many stations and their locations were needed to determine this A value, the A value was calculated for a range of different station configurations. The A value which is calculated using all available stations in the study (45 sensors) is considered the correct value, and the A value calculated with other configurations are compared to this correct value. After testing multiple configurations on several representative days, the number of sensors recommended is five. The days tested were chosen so that a range of A-values and Variability Indexes were tested. The sensors should be located in a X pattern as shown in Figure 4.27. The north-south or east-west distance between adjacent corner sensors should be approximately 700 meters (for example from station 5 to 25 and 25 to 21 in the grid shown in Figure 4.27). Note, in this case station 6 is chosen instead of station 1 because this sensor tended to have less data quality issues than sensor 1.

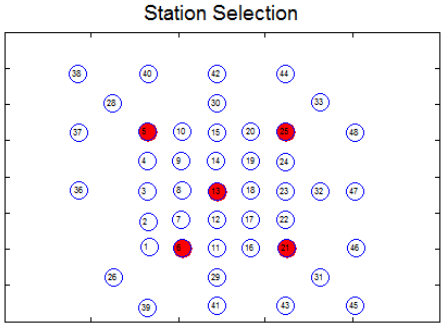

Figure 4.27: A sensor network consisting of five sensors in an X pattern with sensors about 700 meters apart on the diagonals is found to estimate the A-value well.

Table 4.7 shows the A-value calculated with all stations ('correct') and the A-value calculated with the five stations ('Approximate'). For reference the VI is also included.

www.manaraa.com

Table 4.7: The A Value which was calculated with all 45 sensors (assumed to be the 'correct' value) is compared to the A value calculated with the five sensor network.

	Correct A value	Approximate A value	VI
9/22/2012	7.14	7.03	12.1
9/7/2012	2.10	2.13	5.8
4/10/2012	26.2	**21.9**	11.2
11/1/2012	16.2	16.9	3.1
6/27/2012	8.88	**10.4**	21.6
11/16/2012	5.74	6.45	10.8
4/25/2013	6.71	6.34	10.7
9/24/2012	9.62	8.87	17.5
10/12/2012	6.5	**7.6**	13.0

For most conditions, the A value calculated with the five stations in the X configuration matched well with the correct A-value. There are three days where the X configuration gave a noticeably different A value (highlighted in the table above). To examine this in further detail we considered the June 27th date. This date had conditions which made it the most difficult to approximate the A value, and so was considered the limiting case. For this date, in order to get the A-value within 0.5 of the correct value, one needs essentially all of the stations (more than 40). This is a significant cost increase over just five sensors. So, it is proposed that if the approximate A value which can be obtained with the X configuration produces results that closely replicate the variability of the day, then the approximate A value (10.4 instead of the correct value of 8.88 in this case) is sufficient. In order to determine if the approximated A values are sufficient, both April 10th and October 12th were tested. Both of these days had an A-value that was more than one off of the correct A value, and these two days represent high A values (April 10th) and low A values (October 12th). The incorrect A value was used in the WVM to determine the smoothing, and

www.manaraa.com

then compared the VI of the smoothed irradiance with the correct A value to the VI of the smoothed irradiance with the incorrect A value. In both cases, the 30 MW plant size was tested because more smoothing occurs in the 30 MW plant than the 10 MW plant. The results are provided in Table 4.8. Since the VI values are very close when using the correct A-value or the approximate A-value, the approximate A value which was found using five sensors in an X configuration is sufficient to represent the variability (per 1 minute VI) in any conditions.

Table 4.8: The WVM was run with both the correct A value and the approximate value to determine how much an incorrect A value would change the final VI results. In the two cases tested the difference in VI was less than 5 %.

	Correct A value	Approx. A value	VI from Correct A value	VI from Approx. A value	% Difference in VI
4/10/2012	26.2	21.9	10.1	9.9	1.9
10/12/2012	6.5	7.6	8.6	9.0	4.7

Based on the testing that was done to determine the five sensor layout, the A value calculated using a subset of sensors corresponding to any other plant size within the footprint of this network would be the same as the A value calculated with 45 sensors or five sensors. Therefore the five sensor recommendation is applicable to plant sizes up to about 65MW because this is the plant size encompassed by the entire grid of stations (508 acres at 8 acre per 1 MW capacity). For plant sizes beyond this, it is expected that the A value would continue to be useful since the WVM uses the A value in Equation 4.3 which is a function of distance between hypothetical sensor locations over the entire power plant. As long as the cloud characteristics are not changing rapidly over the plant area, the A value determined from five sensors is expected to be applicable to any plant size. Testing with a larger network of sensors

www.manaraa.com

could confirm this.

4.3.3 Temporal sampling: Variability reductions as an indicator of required temporal sampling

The final question of interest in this study was: What is the temporal sampling rate needed to accurately represent the irradiance variability of a solar PV power plant? The time step of irradiance measurements in this study was 1-second. This is atypical; a more common sampling rate is one minute (although sub-sampling under one minute is common). To limit data collection and instrumentation costs while adequately representing the short term variability of irradiance, it is desired to determine what the maximum allowable sampling rate is.

One way to consider the timescale effects of smoothing is by looking at the Variability Reduction (VR) by timescale for a given date. The WVM calculates a VR at each timescale for each day. The VR is calculated from the correlation of irradiance changes at each timescale, which in turn depend on the A value for a given condition. For example, a large VR at two seconds indicates that the changes in irradiance on a timescale of two seconds are greatly smoothed over the plant area. However, a small VR at two seconds indicates that the changes in irradiance are not significantly smoothed over the area. The magnitude of the VR values at each timescale for the most extreme variability days with the least smoothing (largest A value) and most smoothing (smallest A value) were considered here.

As for spatial sampling, the dates of April 10th, 2012, and October 12th, 2012 are considered. Figure 4.28a shows the VR values which are output from the WVM. The VR values are much smaller for the highly correlated day, April 10th. Figure 4.28b

www.manaraa.com

provides more detail for the short timescales of interest.

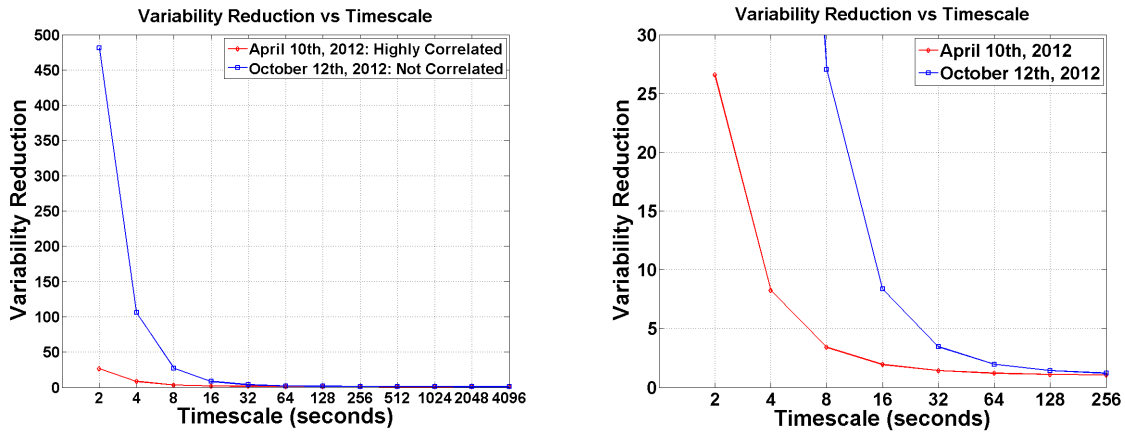

(a) VR (b) VR detail view

Figure 4.28: A comparison of the Variability Reduction for two days with different A-values shows that although the two-second changes are greatly reduced (high VR) for a day with a low A-values, for a day with a high A-value, the two-second changes are not greatly reduced (low VR).

The VR value at two seconds for April 10th is small compared to the values for October 12th (the magnitude is 480, not shown). The VR's impact on the smoothed irradiance is that the wavelet subsignal at the each timescale is divided by the square root of the VR at that timescale. Thus for the October 12th day, this has an impact of reducing the two second subsignal by over 95% (virtually eliminating its impact) but for the April 10th day the two second subsignal is reduced by about 80%. At four seconds the reduction is less (65%).

Although these VR values indicate significant reductions in the short timescale changes, they are not completely wiped out. Since these short timescales are important for system planning (particularly on a sub-regulation level at the distribution system), it is recommended that the 1-second irradiance sampling is maintained.

It is worth noting that the 1-second timescale is important for the single sensor

www.manaraa.com

that will be used as the direct input to the WVM. However, if a sensor network is used to determine the A value, the time resolution could be relaxed. Since the A value determined from the network of sensors is based off of a best fit line to a relationship that includes the term $exp^{\left(\frac{-d_{m,n}}{t}\right)}$, as long as there are a number of different distances and timescales included in the dataset to fit the model to, it is likely not necessary to have a temporal sampling of one second on the sensor network.

www.manaraa.com

Chapter 5

Conclusion

This thesis used the Wavelet Variability Model to predict the spatial smoothing of irradiance over the area of large-scale PV power plants. The irradiance dataset employed was from a dense network of irradiance sensors measuring irradiance at one-second resolution over 18 months. The work completed with the aim of predicting spatial smoothing included a review of solar variability and spatial smoothing literature, selection of relevant metrics and analysis methods, quality control of the dataset, and, finally, implementation of variability analysis and the WVM, which ultimately allowed for analysis of the spatial smoothing.

The results of the work provide answers to the three basic research questions posed related to spatial smoothing. Those questions and the pertinent results and conclusions are:

www.manaraa.com

What is the smoothing of the irradiance profile from a single point irradiance measurement to the integrated irradiance over the area of a solar PV power plant of distribution scale and of transmission scale?

- The WVM uses the correlation scaling coefficient (A), which is proportional to cloud speed, to model the smoothing of irradiance over the power plant. The magnitude of the A value indicates the extent of the smoothing. For the 28 days examined in detail in this study, it was found that for clear days (daily one-minute VI approximately one), the smoothing over the area of the plant for either a transmission scale or distribution scale plant is negligible due to the negligible variations in the irradiance on a clear day. However for more variable days, the A value dictates the smoothing extent. Using the percent decrease in daily one-minute VI as a measure of the smoothing, it was found that for low A values (less correlated stations/lower cloud speeds), the smoothing results in an up to to 60% decrease in VI. For days with higher A values (more correlated stations), the smoothing would only result in a 10 to 20% decrease in VI. Although this result is not surprising, it is important to understand the effect that A value has if the model is adopted for solar variability studies which cover longer periods of time. It is key to understand that high variability days, which are of most concern to system planners, could be characterized by either high A values (little smoothing will occur) or low A values (smoothing will be significant), or anything in between.

- For a distribution scale power plant (10MW was the selected size) the WVM model decreased the average daily VI over the highly variable period from 25.2

www.manaraa.com

to 20.2. The irradiance ramps detected over this period decreased from 11,324 ramps with a single point sensor to 3,924 ramps. It was significant that the very short duration ramps were eliminated with the WVM model. Specifically, for this high VI period, while the single point sensor irradiance had many one second ramps, the 10MW WVM simulation had no ramps shorter than three seconds. The mean ramp duration was 26 seconds for a single sensor and 75 seconds for the 10MW WVM model. This is consistent with a 'smoothing' or 'spreading out' of ramps due to cloud movement over sensors - the shortest ramps are not observed but instead are incorporated into longer ramps. Thus when comparing the magnitudes of the longer ramps, the magnitudes are larger with the WVM simulation. For example it was found that the magnitudes of the 95th percentile ramp magnitudes for durations from 10-20 seconds long were slightly more with the WVM model than the single point sensor. The regulation ramps detected were similar between the single point sensor irradiance and the WVM model, suggesting that if the regulation timescale is of interest for a particular application, it would not be necessary to implement the WVM to predict the regulation effects. The sub-regulation ramp distributions were smoothed in a manner similar to the irradiance ramps except for that the very shortest duration ramps were not eliminated. In either the point irradiance or 10MW WVM sub-regulation timeseries, the algorithm did detect one second ramps. These smoothing effects mean the power plant output would have less variability and would be easier to integrate into the electricity grid than might have been expected using a single point sensor measurement to predict variability.

www.manaraa.com

- For a transmission scale power plant (30MW was the selected size here) the WVM model decreased the average daily VI over the highly variable period from 25.2 to 17.8. The irradiance ramps detected over this period decreased from 11,324 ramps with a single point sensor to 3,037 ramps. Again the very short duration ramps were eliminated with the WVM model. For the 30 MW plant, for this high VI period, while the single point sensor irradiance detected many 1-second ramps, the 30MW WVM simulation had no ramps shorter than four seconds. The mean ramp duration was 26 seconds for a single sensor and 96 seconds for the 30 MW WVM model. The ramp distributions of the 30 MW WVW model were generally consistent with the 10 MW model but showing more smoothing as expected over the larger area. Again, these smoothing effects are positive from the perspective of grid integration of solar PV.

- The WVM results were compared to an aggregate model which used an average of the irradiance measured at either nine sensors in the network (for 10MW plant size) or 25 sensors (for 30MW plant size). The two models predicted smoothing differently, with the WVM in general predicting more smoothing (lower smoothed VI values, fewer ramp events). While the WVM model greatly reduced the ramps under about five seconds in duration, the aggregate model detected 1-5 second ramp events. The aggregate model was also found to be more prone to sensor or datalogger malfunction, which caused an anti-smoothing effect during very clear summer periods. While this is not extremely troubling because the variability during these clear days is extremely small no matter how it is modeled, it does point out some benefits of the WVM. Although validation against actual power plant output was not possible at this site, the

www.manaraa.com

WVM's prediction of fewer, longer ramps would be more favorable from a grid integration perspective and so is a promising result.

How many irradiance sensors are required to predict the smoothing of distribution-scale and transmission-scale power plants using wavelet-based variability analysis? What is the ideal layout of those sensors?

The WVM predicts smoothed irradiance using single point sensor irradiance, and A value, and the power plant location and footprint. Since the A value is the only relevant model input that depends on the number of sensors, various sub-sets of the 45 sensors available were tested to determine how many sensors and in what configuration would minimize the data collection cost while maintaining the modeled irradiance variability. A network of five sensors in an 'X' configuration was found to adequately predict the A value such that the WVM modeled irradiance would maintain the correct variability as measured by 1-minute daily VI. The five sensors should be placed with a distance of approximately 700 meters from adjacent corners. This configuration is usable for plant sizes up to about 65 MW, and may be useable beyond that scale as well, although the data used for this work cannot validate this extension. Although the focus of this study was on using the dense network of irradiance sensors to implement the WVM and predict smoothing, in reality it has been shown that the A value can be determined from cloud speed measurements instead of a sensor network [22], thus eliminating the need for anything but a single point sensor measurement, assuming cloud speeds are available.

www.manaraa.com

What temporal sampling rate is required to capture the variability of distribution scale and transmission scale power plants?

The WVM algorithm uses a variability reduction (VR) value, which is a function of plant size and timescale, to implement the smoothing at each timescale. A high VR value at a certain timescale would indicate that the irradiance changes at that timescale are smoothed out over the area of the power plant. Since the WVM calculates and outputs VR at each of the diatic timescales used in the model, these outputs were used to determine temporal sampling requirements. Two different days with different irradiance characteristics were examined. Although the VR is greatest at the short timescales, the VR values are not large enough to indicate that the short timescales can be ignored all together. A one second irradiance measurement is therefore recommended to use the WVM to model spatial smoothing. However, it is expected that only one sensor need record 1-second data, while the sensor network used to determine the A value (if a network exists) could use higher sampling intervals.

Next questions

During the course of completing this work, several related questions came to light that would be valuable in the study of spatial smoothing for large solar PV power plants.

- This unique sensor network could be used to validate cloud speeds estimates made from numerical weather prediction models. The network could be used to determine A values (as was done for this study) and then those A values could be related to cloud speed per Lave and Kleissl [22].

www.manaraa.com

- A longer period of analysis could be used to examine how the A value changes throughout the year in this location. This would allow more generalizations to be made about the spatial smoothing at this location, instead of just examining the four representative variability categories.

- The spatial sampling question could be approached from an optimization point of view, wherein the configuration and number of sensors could be adjusted to optimize model accuracy and data collection cost in a methodological way. Moreover, a geostatistical modeling technique called kriging, which was also used as part of the larger NextEra project, could be used to provide granularity to the irradiance measurements. This could improve the optimization because the sensor locations would not be limited to the exact 45 locations which were available in this study.

- The WVM and variability analysis techniques used here could be validated by repeating the analysis at locations which have existing power plants. This would allow for comparisons between the WVM smoothed irradiance and the actual power plant output. Since the variability of the actual power output is what is important, these validations would be of interest. (In fact, this has already been done by Lave and Kleissl [31], but independent validations would be valuable).

- Variability measured at this site was limited to the one-second time resolution of the data. The analysis could be completed for sub-second data to determine if any variability effects at these timescales are important and if to what extent spatial smoothing occurs at these timescales.

www.manaraa.com

Bibliography

[1] Matthew Lave, Jan Kleissl, and Joshua S Stein. A Wavelet-based Variability Model (WVM) for Solar PV Power Plants. *Sustainable Energy, IEEE Transactions*, 4(2):501–509, 2013.

[2] U.S. Energy Information Administration. Annual Energy Review 2011 DOE/EIA-0384. Technical report, Department of Energy, 2012.

[3] U.S. Energy Information Administration. Monthly Energy Review September 2013 DOE/EIA-0035(2013/09). Technical report, U.S. Energy Information Administration, 2013.

[4] Annual Energy Outlook 2013 With Projections to 2040 DOE/EIA-0383(2013). Technical report, U.S. Energy Information Administration, 2013.

[5] Thomas E Hoff and Richard Perez. Modeling PV fleet output variability. *Solar Energy*, 84(10):1–20, 2011.

[6] Andrew Mills and Ryan Wiser. Implications of Wide-Area Geographic Diversity for Short- Term Variability of Solar Power LBNL-3884E. Technical Report September, Ernest Orlando Lawrence Berkeley National Laboratories, 2010.

www.manaraa.com

[7] John Duffie and William Beckman. *Solar Engineering of Thermal Processes*. Wiley, 1991.

[8] Matthew J Reno, Clifford W Hansen, and Joshua S Stein. Global Horizontal Irradiance Clear Sky Models: Implementation and Analysis SAND2012-2389. Technical Report March, Sandia National Laboratories, 2012.

[9] Pierre Ineichen. Comparison of eight clear sky broadband models against 16 independent data banks. *Solar Energy*, 80(4):468–478, April 2006.

[10] Joshua S Stein, Matthew J Reno, and Clifford W Hansen. The Variability Index: A New and Novel Metric for Quantifying Irradiance and PV Output Variability. Technical report, Sandia National Laboratories, 2012.

[11] Ronald K. Flood, Tom Acker, David Willy, Jeff Lerner, and Amy Vandervoort. Prescott Airport Solar Facility Solar Variability Study. Technical report, Arizona Public Services, Northern Arizona University, 3Tier, Inc., 2011.

[12] David Willy. *Power output variability and metrics for utility-scale solar photovoltaics power plant*. Master's thesis, Northern Arizona University, 2012.

[13] Rob van Haaren, Mahesh Morjaria, and Vasilis Fthenakis. Empirical assessment of short-term variability from utility-scale solar PV plants. *Prog. Photovolt: Res. Appl.*, 2012.

[14] A Longhetto, G Elisei, and C Giraud. Effect of correlations in time and spatial extent on performance of very large solar conversion systems. *Solar Energy*, 43(2):77–84, 1989.

www.manaraa.com

[15] Joshua S. Stein, Abraham Ellis, and Clifford W. Hansen. Simulation of one-minute power output from utility-scale photovoltaic generation systems, SAND2001-5529. Technical report, Sandia National Laboratories (SNL), Albuquerque, NM, and Livermore, CA (United States), August 2011.

[16] Javier Marcos, Luis Marroyo, Eduardo Lorenzo, and Miguel García. Smoothing of PV power fluctuations by geographical dispersion. *Prog. Photovolt: Res. Appl.*, 20(July 2011):226–237, 2012.

[17] Kenji Otani, Jyunya Minowa, and Kosuke Kurokawa. Study on areal solar irradiance for analyzing areally-totalized PV systems. *Solar Energy Materials and Solar Cells*, 47, 1997.

[18] Matthew Lave and Jan Kleissl. Solar variability of four sites across the state of Colorado. *Renewable Energy*, 35(12):2867–2873, December 2010.

[19] Matthew Lave, Jan Kleissl, and Ery Arias-Castro. High-frequency irradiance fluctuations and geographic smoothing. *Solar Energy*, 86(8):2190–2199, August 2012.

[20] Scott Kuszamaul, Abraham Ellis, Joshua Stein, and Lars Johnson. Lanai High-density Irradiance Sensor Network for Characterizing Solar Resource Variability of MW-scale PV System. In *IEEE Photovoltaic Specialists Conference*, pages 4–9, Honolulu, HI, 2010.

[21] Javier Marcos, Luis Marroyo, Eduardo Lorenzo, David Alvira, and Eloisa Izco. From irradiance to output power fluctuations: the pv plant as a low pass filter. *Prog. Photovolt: Res. Appl.*, 19(January):505–510, 2011.

www.manaraa.com

[22] Matthew Lave and Jan Kleissl. Cloud Speed Impact on Solar Variability Scaling - Application to the Wavelet Variability Model. *Solar Energy*, 91:11–21, 2013.

[23] Clifford W Hansen, Joshua S Stein, and Daniel Riley. Effect of Time Scale on Analysis of PV System Performance, SAND2012-1099. Technical Report February, Sandia National Laboratories, 2012.

[24] Daniel M Riley, Christopher P Cameron, Joshua A Jacob, Jennifer E Granata, and Gary M Galbraith. Quantifying the Effects of Averaging and Sampling Rates on PV. In *Phtovoltaic Specialists Conference, 2009 34th IEEE*, pages 456–461, Philadelphia, PA, 2009.

[25] Donald Percival and Andrew Walden. *Wavelet Methods for Time Series Analysis*. Press Syndicate of the University of Cambridge, 2000.

[26] Norihiro Kawasaki, Takashi Oozeki, Kenji Otani, and Kosuke Kurokawa. An evaluation method of the fluctuation characteristics of photovoltaic systems by using frequency analysis. *Solar Energy Materials and Solar Cells*, 90(18-19):3356–3363, November 2006.

[27] Achim Woyte, Ronnie Belmans, and Johan Nijs. Fluctuations in instantaneous clearness index: Analysis and statistics. *Solar Energy*, 81(2):195–206, February 2007.

[28] Pierre Ineichen and Richard Perez. A New Airmass Independent Formulation for the Linke Turbidity Coefficient. *Solar Energy*, 73(3):151–157, 2002.

[29] LI-COR. LI-COR Terrestrial Radiation Sensors Instruction Manual, 2005.

www.manaraa.com

[30] Jan Remund, Lucien Wald, Mireille Lefevre, Thierry Ranchin, and John Page. Worldwide Linke Turbidity Information. In *Proc. ISES Solar World Congress*, Goteborg, Sweden, 2003.

[31] M Lave and J Kleissl. Testing a Wavelet-based Variability Model (WVM) for Solar PV Power Plants. *Power and Energy Society General Meeting, IEEE*, pages 1–6, 2012.

www.manaraa.com

Appendix A

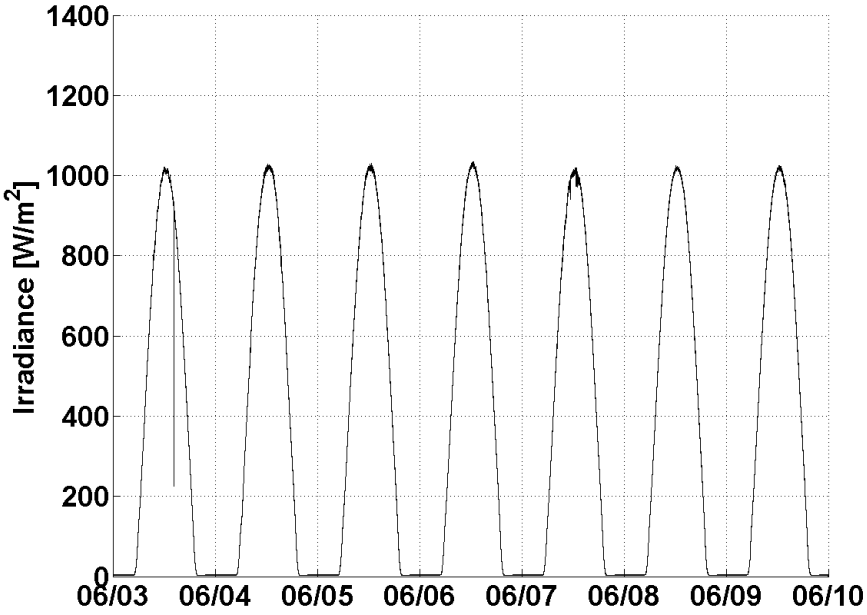

Figure A.1: The irradiance over the seven day Very Low VI period shows that the sky was almost completely clear.

www.manaraa.com

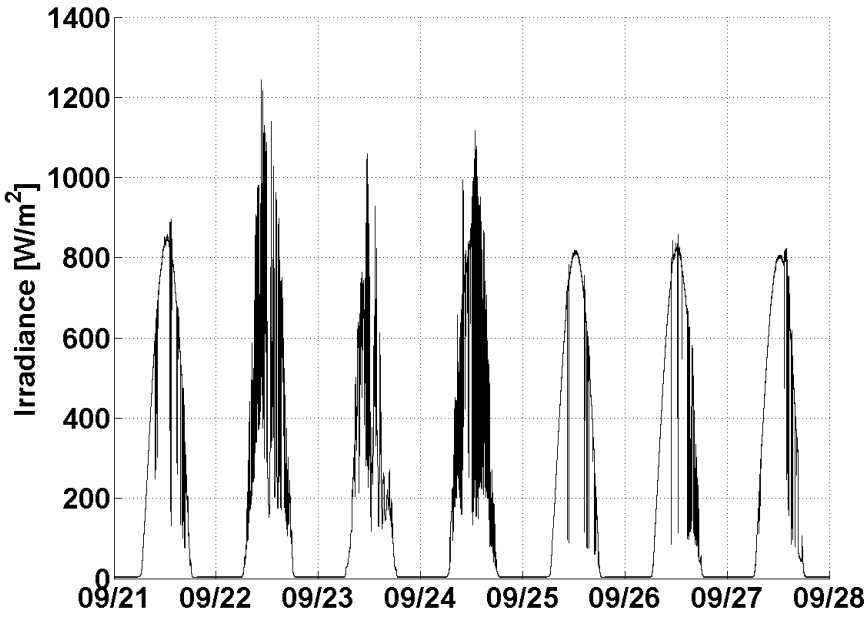

Figure A.2: The irradiance during the Low VI period (September) shows that the period included conditions from clear to variable.

www.manaraa.com

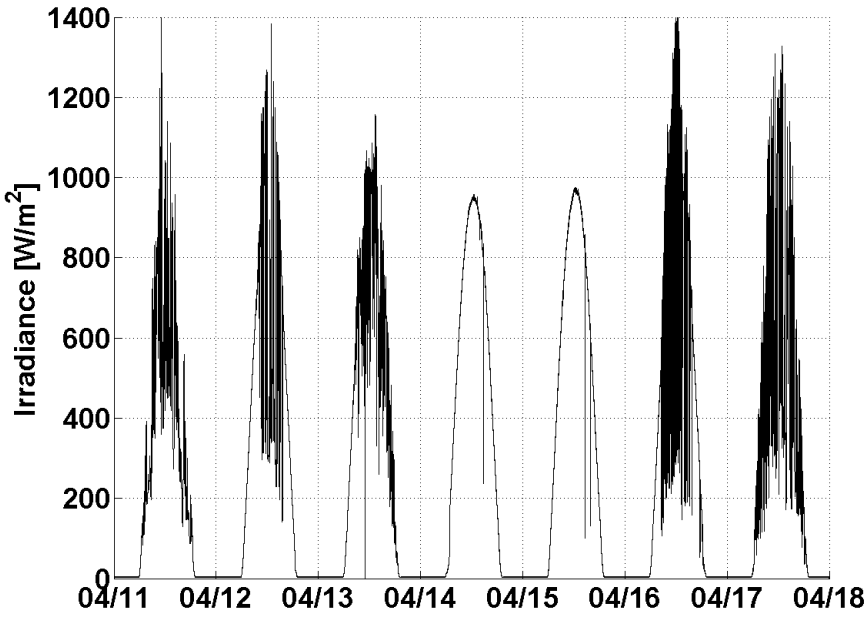

Figure A.3: The irradiance during the Medium VI period shows that the period included five variable days and two clear days.

www.manaraa.com

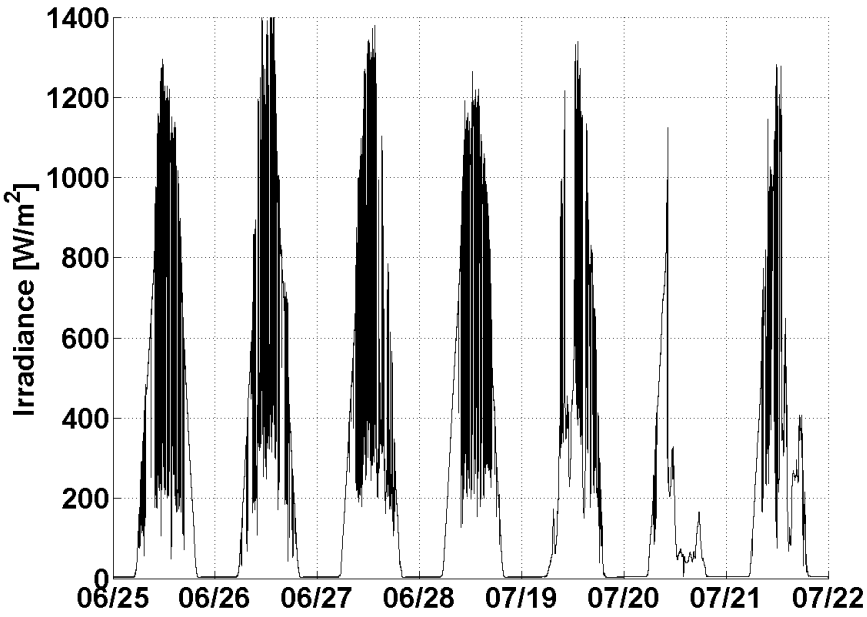

Figure A.4: The irradiance during the High VI period included no clear days and several very high variability days during the monsoon season.

Table A.1: Irradiance ramp statistics for the Very Low VI Period show few ramps detected regardless of the smoothing method used.

		Number of Ramps	Standard Deviation of Absolute Value	Mean of Absolute Value	Minimum	Maximum	95th Percentile of Absolute Values	99th Percentile of Absolute Values	99.5th Percentile of Absolute Values
Single Station	Duration [sec]	87	3,718.9	3,627.9	2	12,546	11,453	12,415	12,546
	Magnitude [W/m^2]	87	179.3	170.4	(525)	652	604	647	652
	Ramp Rate [W/m^2/sec]	87	15.7	6.6	(68)	78	43	74	78
10 MW Agg	Duration	296	2,413.1	1,066.3	1	11,238	6,812	10,733	11,210
	Magnitude	296	102.5	73.8	(564)	633	291	577	609
	Ramp Rate	296	30.4	21.6	(119)	116	94	115	119
30 MW Agg	Duration	522	1,576.7	604.7	1	9,141	4,538	7,890	8,462
	Magnitude	522	67.7	40.9	(479)	414	156	392	448
	Ramp Rate	522	9.9	7.3	(41)	34	29	34	34
10 MW WVM	Duration	42	3,244.0	7,515.0	182	12,903	12,814	12,903	12,903
	Magnitude	42	235.6	283.4	(613)	668	662	668	668
	Ramp Rate	42	0.0	0.0	(0)	0	0	0	0
30 MW WVM	Duration	42	3,426.2	7,515.0	191	12,875	12,801	12,875	12,875
	Magnitude	42	242.8	281.0	(617)	668	663	668	668
	Ramp Rate	42	0.0	0.0	(0)	0	0	0	0

www.manaraa.com

Table A.2: Irradiance ramp statistics for the Low VI Period show the WVM predicts fewer, longer ramps than the aggregate model.

		Number of Ramps	Standard Deviation of Absolute Value	Mean of Absolute Value	Minimum	Maximum	95th Percentile of Absolute Values	99th Percentile of Absolute Values	99.5th Percentile of Absolute Values
Single Station	Duration [sec]	4943	356.1	51.8	1	9,916	144	685	1,440
	Magnitude [W/m^2]	4943	70.4	83.0	(518)	497	221	314	345
	Ramp Rate [W/m^2/sec]	4943	48.1	29.0	(518)	343	133	225	264
10 MW Agg	Duration	4047	331.1	63.3	1	7,393	198	784	1,398
	Magnitude	4047	46.9	53.6	(294)	354	149	223	241
	Ramp Rate	4047	14.3	9.2	(109)	113	40	65	76
30 MW Agg	Duration	2191	437.8	116.9	1	9,170	439	1,440	3,068
	Magnitude	2191	55.7	55.8	(407)	414	169	263	315
	Ramp Rate	2191	5.1	3.3	(45)	38	13	27	31
10 MW WVM	Duration	1939	589.6	132.1	3	10,583	425	1,931	4,405
	Magnitude	1939	62.7	78.3	(364)	521	200	283	327
	Ramp Rate	1939	7.3	4.8	(52)	46	21	35	42
30 MW WVM	Duration	1457	567.0	150.8	5	10,128	509	2,140	4,149
	Magnitude	1457	59.2	76.5	(319)	507	189	252	312
	Ramp Rate	1457	4.8	3.3	(30)	27	14	23	25

Table A.3: Irradiance ramp statistics for the Medium VI Period show the WVM predicts fewer, longer ramps than the aggregate model.

		Number of Ramps	Standard Deviation of Absolute Value	Mean of Absolute Value	Minimum	Maximum	95th Percentile of Absolute Values	99th Percentile of Absolute Values	99.5th Percentile of Absolute Values
Single Station	Duration [sec]	11487	241.2	23.3	1	9,356	49	249	511
	Magnitude [W/m^2]	11487	84.2	91.8	(763)	638	256	404	451
	Ramp Rate [W/m^2/sec]	11487	85.6	59.8	(763)	638	242	390	439
10 MW Agg	Duration	9915	256.1	28.5	1	9,786	73	308	536
	Magnitude	9915	50.0	62.9	(553)	523	157	221	255
	Ramp Rate	9915	32.2	25.6	(255)	248	95	140	156
30 MW Agg	Duration	7616	251.5	37.1	1	9,184	104	459	907
	Magnitude	7616	44.3	52.4	(359)	511	138	205	237
	Ramp Rate	7616	16.7	13.0	(136)	99	49	73	84
10 MW WVM	Duration	3345	522.6	84.5	1	10,785	174	775	2,307
	Magnitude	3345	63.8	79.8	(507)	624	194	278	328
	Ramp Rate	3345	7.3	5.0	(119)	122	18	27	34
30 MW WVM	Duration	2572	593.0	110.0	2	10,801	230	942	5,384
	Magnitude	2572	63.5	78.7	(500)	629	192	285	329
	Ramp Rate	2572	4.2	3.2	(59)	62	11	16	21

Table A.4: Irradiance ramp statistics for the High VI Period show the WVM predicts fewer, longer ramps than the aggregate model.

		Number of Ramps	Standard Deviation of Absolute Value	Mean of Absolute Value	Minimum	Maximum	95th Percentile of Absolute Values	99th Percentile of Absolute Values	99.5th Percentile of Absolute Values
Single Station	Duration [sec]	11324	188.5	25.8	1	8,155	70	410	743
	Magnitude [W/m^2]	11324	80.3	94.6	(1,154)	1,139	237	349	403
	Ramp Rate [W/m^2/sec]	11324	62.2	44.1	(1,154)	1,139	156	248	289
10 MW Agg	Duration	8329	234.7	35.1	1	15,289	97	561	1,009
	Magnitude	8329	52.6	64.8	(417)	441	169	234	259
	Ramp Rate	8329	13.8	10.7	(156)	166	36	62	80
30 MW Agg	Duration	5931	271.9	49.3	1	15,280	153	705	1,277
	Magnitude	5931	46.0	53.6	(506)	315	140	209	235
	Ramp Rate	5931	6.2	4.9	(55)	75	16	27	33
10 MW WVM	Duration	3924	330.8	74.5	3	11,372	236	1,110	1,876
	Magnitude	3924	69.9	93.5	(452)	414	235	320	344
	Ramp Rate	3924	8.2	6.8	(56)	49	24	37	42
30 MW WVM	Duration	3037	375.8	96.3	4	11,353	307	1,486	2,223
	Magnitude	3037	67.2	92.0	(386)	373	224	304	324
	Ramp Rate	3037	5.5	4.6	(34)	30	17	25	27

www.manaraa.com